SANDIA REPORT

SAND2009-4440
Unlimited Release
Printed July 2009

Nanostructural Engineering of Nitride Nucleation Layers for GaN Substrate Dislocation Reduction

D. D. Koleske, S. R. Lee, M. E. Coltrin, G. Thaler, K. C. Cross, and T. K. Lemp

Prepared by
Sandia National Laboratories
Albuquerque, New Mexico 87185 and Livermore, California 94550

Sandia is a multiprogram laboratory operated by Sandia Corporation,
a Lockheed Martin Company, for the United States Department of Energy's
National Nuclear Security Administration under Contract DE-AC04-94AL85000.

Issued by Sandia National Laboratories, operated for the United States Department of Energy by Sandia Corporation.

Available to DOE and DOE contractors from
U.S. Department of Energy
Office of Scientific and Technical Information
P.O. Box 62
Oak Ridge, TN 37831

Telephone: (865)576-8401
Facsimile: (865)576-5728
E-Mail: reports@adonis.osti.gov
Online ordering: http://www.osti.gov/bridge

Available to the public from
U.S. Department of Commerce
National Technical Information Service
5285 Port Royal Rd
Springfield, VA 22161

Telephone: (800)553-6847
Facsimile: (703)605-6900
E-Mail: orders@ntis.fedworld.gov
Online order: http://www.ntis.gov/help/ordermethods.asp?loc=7-4-0#online

SAND2009-4440
Unlimited Release
Printed July 2009

Nanostructural Engineering of Nitride Nucleation Layers for GaN Substrate Dislocation Reduction

D. D. Koleske
Advanced Material Sciences Department

S. R. Lee
Semiconductor Material & Device Sciences Department

M. E. Coltrin, G. Thaler, K. C. Cross
Advanced Material Sciences Department

and

T. K. Lemp
MESAFab Engineering Department

Sandia National Laboratories
P.O. Box 5800
Albuquerque, New Mexico 87185-1086

Abstract

With no lattice matched substrate available, sapphire continues as the substrate of choice for GaN growth, because of its reasonable cost and the extensive prior experience using it as a substrate for GaN. Surprisingly, the high dislocation density does not appear to limit UV and blue LED light intensity. However, dislocations may limit green LED light intensity and LED lifetime, especially as LEDs are pushed to higher current density for high end solid state lighting sources. To improve the performance for these higher current density LEDs, simple growth–enabled reductions in dislocation density would be highly prized.

GaN nucleation layers (NLs) are not commonly thought of as an application of nano-structural engineering; yet, these layers evolve during the growth process to produce self-assembled, nanometer-scale structures. Continued growth on these nuclei ultimately leads to a fully coalesced film, and we show in this research program that their initial density is correlated to the GaN dislocation density.

In this 18 month program, we developed MOCVD growth methods to reduce GaN dislocation densities on sapphire from $5x10^8$ cm^{-2} using our standard delay recovery growth technique to $1x10^8$ cm^{-2} using an ultra-low nucleation density technique. For this research, we firmly established a correlation between the GaN nucleation thickness, the resulting nucleation density after annealing, and dislocation density of full GaN films grown on these nucleation layers. We developed methods to reduce the nuclei density while still maintaining the ability to fully coalesce the GaN films. Ways were sought to improve the GaN nuclei orientation by improving the sapphire surface smoothness by annealing prior to the NL growth. Methods to eliminate the formation of additional nuclei once the majority of GaN nuclei were developed using a silicon nitride treatment prior to the deposition of the nucleation layer. Nucleation layer thickness was determined using optical reflectance and the nucleation density was determined using atomic force microscopy (AFM) and Nomarski microscopy. Dislocation density was measured using X-ray diffraction and AFM after coating the surface with silicon nitride to delineate all dislocation types. The program milestone of producing GaN films with dislocation densities of $1x10^8$ cm^{-2} was met by silicon nitride treatment of annealed sapphire followed by the multiple deposition of a low density of GaN nuclei followed by high temperature GaN growth. Details of this growth process and the underlying science are presented in this final report along with problems encountered in this research and recommendations for future work.

Acknowledgments

We acknowledge the daily technical contributions to the growth and characterization of the GaN films and routine maintanence of the MOCVD growth equipment by Jeff Figiel and Mike Russell. We also acknowledge Mike Russell for prior technical contributions on the older MOCVD reactor which layed the foundation for understanding the GaN nucleation evolution.

Sandia is a multiprogram laboratory operated by Sandia Corporation, a Lockheed Martin Company. This work is supported by the Division of Material Science, Office of Basic Energy Science for the United States Department of Energy's National Nuclear Security Administration under Contract DE-AC04-94AL85000.

Contents

Figures List

Tables List

Nomenclature

AFM	atomic force microscopy
AlN	aluminum nitride
d_{NL}	initial GaN nucleation layer thickness
DOE	Department of Energy
ELOG	epitaxial lateral overgrowth
EQE	external quantum efficiency
GaN	gallium nitride
H_2	hydrogen gas
H_20	water
HBA	hazard barrier analysis
IQE	internal quantum efficiency
LED	light emitting diode
μmoles	micromoles
μm	micrometer
MOCVD	metalorganic chemical vapor deposition
NH_3	ammonia gas
n or n_D	nuclei density or nucleation density
N_2	nitrogen gas
NL	nucleation layer
nm	nanometer
sccm	standard cubic centimeters per minute
PSD	power spectral density (from AFM measurement)
ρ	dislocation density
RMS	root-mean-square
SEM	scanning electron microscope
Si	elemental silicon
SiC	silicon carbide
SiN	silicon nitride
SLM	standard liters per minute
SNL	Sandia National Laboratories
SSL	solid state lighting
TEM	transition electron microscopy
TMGa	trimethylgallium
UV	ultra-violet
VTD	vertical threading dislocations
XRD	x-ray diffraction

0. Executive Summary

Despite the success in the growth and fabrication of bright blue and green LED using the group III nitrides, GaN substrates for manufacture of these devices do not exist. Instead, as part of the growth process, GaN must be grown on foreign substrates such as sapphire or silicon carbide. These foreign substrates do not have the same lattice constants as the GaN grown on top of it and as a result the GaN has many defects. These defects called dislocations develop in the GaN film as it grows to accommodate the lattice constant mismatch between the foreign substrate and the GaN film.

Surprisingly, for the group III nitrides these dislocations which number in the $10^8 - 10^9$ cm^{-2} do not entirely negate the light emission eminating from nitride-based LEDs. If LEDs were fabricated on the group III arsinides or phosphides with this same high level of dislocation, no light would be produced. The exact reason why dislocations in the group III nitrides are not as detrimental to producing light is still not thoroughly understood, however, phenonema which localize the electron and holes away from the dislocations are larger in the group III nitrides compared to the other group III arsinides or phosphides.

Although the LEDs fabricated on the existing high dislocation density GaN films work well allowing record breaking achievements in both IQE and EQE of blue LEDs, this research adds to our general understanding of dislocation density reduction in heteroepitaxial growth systems. The development of controlling and understanding the details of the GaN heteroepitaxial growth system should aid in the growth of future materials systems, as these new materials systems are unlikely to have a lattice matched substrate suitable for growth. For the present program reduced dislocation density GaN templates should improve the growth of LED structures and thereby improving LEDs for solid state lighting. Improved GaN films with fewer dislocations will especially improve green nitride-based LEDs by reducing the number of V-defects which form on threading dislocation during the growth of these high indium content LEDs.

Economically, sapphire is chosen as a substrate for GaN growth not because is is particularly well suited for GaN growth, but because it is relatively inexpensive and much experience has been gained over the years on how to grow GaN on it. Prior to 1985, GaN was grown on sapphire at high temperature resulting in material with dislocation densities > 10^{10} cm^{-2}, rendering the material useless for LEDs. In 1985 Amano *et al.* used a thin AlN nucleation layer (NL) to bridge to difference in the lattice constants between GaN and sapphire, and thereby reducing the dislocation density to ~$1x10^9$ cm^{-2}. Later in 1991, both Shuji Nakamura and Dennis Wickenden demonstrated the same benefit using low-temperature GaN NL to achieve dislocation densities of ~$1x10^9$ cm^{-2}. The invention of the NL to improve GaN heteroepitaxial growth on sapphire was one of the developments in the early 1990's that made possible the steady improvement witnessed today in GaN-based LEDs. Although suitably bright blue LEDs can be grown on GaN films with ~$1x10^9$ cm^{-2}, there is mounting evidence to suggest that improvements in green LEDs and high power LEDs might benefit from GaN films with lower dislocation densities.

The research conducted in this program aims to improve the understanding of how GaN NLs can be nano-engineered to further reduce GaN dislocation densities on sapphire. Although not generally viewed as an example of self-assembled nanotechnology, we shall show that the evolved GaN NLs form nanometer sized nuclei whose spacing and size is governed by the MOCVD growth conditions. *The major goal of this proposal is to use nanoscale engineering of the GaN nuclei to achieve lower dislocation GaN substrates for improved LED lifetime and potentially brighter green LEDs.* In this program we demonstated that dislocation densities of $1x10^8$ cm^{-2} or lower can be routinely obtained with out too much additional processing expense, provided that several key factors in the NL growth and the nuclei formation, evolution, and coalescence are better understood. To answer these questions we will investigate the following tasks in this program:

- Determine the correlation between nanoscale GaN nuclei density and resultant dislocation density in GaN full films.
- Develop techniques to reduce the GaN nuclei density and subsequent dislocation density. These will include varying the GaN nucleation layer thickness and annealing schedules to produce lower nuclei densities. After the GaN grains are established, SiN auto masking will be used to prevent the formation of additional GaN nuclei and to minimize the interaction between the laterally coalescing GaN grains and the sapphire substrate.
- Develop sapphire conditioning procedures to vary the sapphire smoothness, including high temperature annealing, nitridation, and in-situ SiN formation. This should improve the GaN nuclei orientation and decrease the degree of misfit that must be accommodated during coalescence.

The work presented here addresses the research area for improvement of internal efficiency of nitride LEDs through the reduction of defects. Specifically, we will use natural self-assembly techniques to produce nanostructures on the surface during the initial stages of epitaxial growth. Using these nanostructures with improved selectivity and improved lateral growth should reduce the dislocation density, leading to improved GaN films on sapphire and potentially nitride-based LEDs that can be run at higher power for increased brightness and efficiency.

1. Project Objective

Nanostructure engineering was used to reduce the dislocation density of GaN films grown by MOCVD on sapphire. This was accomplished by reducing the GaN nanoscale nucleation density, thereby reducing the GaN dislocation density. Methods were developed to reduce nucleation density and to prevent parasitic nucleation of additional GaN nuclei during full film coalescence. Methods were also developed to improve the GaN nuclei orientation on the sapphire surface to further reduce the amount of grain misorientation that must be accommodated during coalescence. Optical reflectance will be used to monitor and control the GaN film evolution.

2. Project Background

Although GaN was first synthesized over 70 years ago [1], the lack of a lattice matching substrate continues to be a challenge for the growth of the group III nitrides; GaN substrates are currently only available in limited quantities. For this reason, GaN is usually grown on sapphire or SiC, not because these substrates are particularly well suited for GaN growth, but because much experience has been gained over the years on how to grow GaN on them. In this section we highlight what was known about the GaN nucleation layer growth and evolution prior to the beginning of this research project.

2.1. GaN nucleation and initial stages of growth

Early on, progress in GaN growth was typically hampered by poor nucleation on sapphire which resulted in large dislocation densities and for many years these high dislocation densities reduced the group III nitrides to a research curiosity and hampered device development. This situation changed with the development of AlN [2] and later GaN [3, 4] nucleation layers. These nanometer thick, low temperature deposited layers help bridge the difference in lattice constant by providing nucleation sites (for growth on AlN) or GaN nuclei on which further growth occurs. The fabrication of UV, blue and green LEDs for SSL is possible today because of the invention and routine use of GaN NLs.

Significantly, the mechanistic details of GaN NL evolution have only recent been uncovered [5]. After the growth of the low temperature GaN NL at ~530 °C, the NL is usually annealed in NH_3

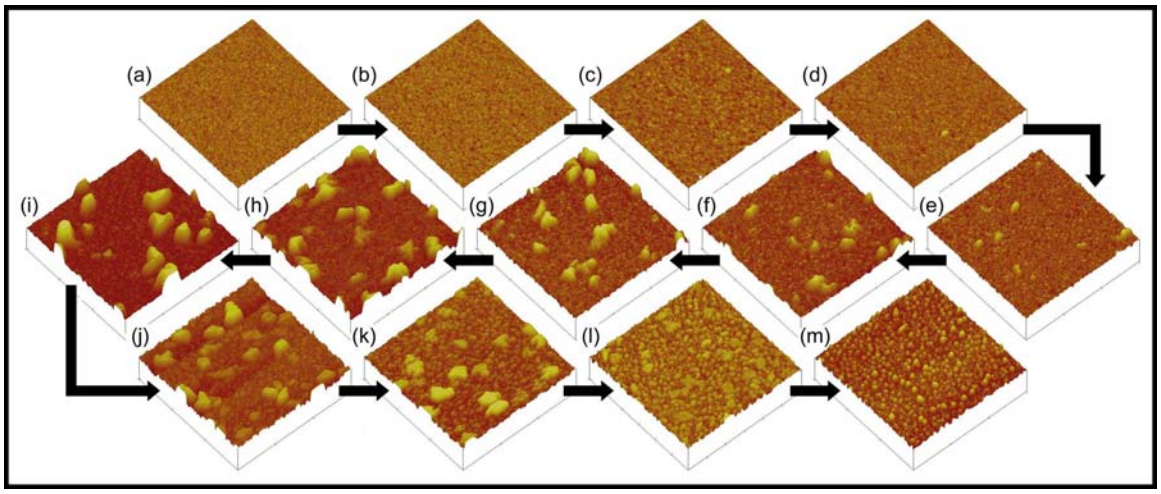

Fig. 1. Atomic force microscopy (AFM) images of the GaN nucleation layer morphology for different annealing temperatures and times. The points (a)-(m) correspond to annealing T and times of (a) 920 °C, (b) 940 °C, (c) 960 °C, (d) 980 °C, (e) 1000 °C, (f) 1020 °C, (g) 1040 °C, (h) 1050 °C, (i) 1050 °C + 1 min., (j) 1050 °C + 2 min., (k) 1050 °C + 3 min., (l) 1050 °C + 5 min., and (m) 1050 °C + 13 min. The arrows indicate the progression along the annealing schedule. The height scale is 200 nm and the scan size is 3 x 3 μm. No change in the AFM morphology occurs on the first row as part of the annealing schedule is dominated by NL decomposition. The second row shows the birth and growth of the high *T* GaN nuclei, and the third row shows the decomposition of the high *T* GaN nuclei. Image taken from Koleske *et al.* Ref. [5].

(also H_2 and N_2) up to ~1050 ºC to begin the high temperature GaN growth. AFM images (3 x 3 μm) of the NL evolution during this annealing process are shown in Fig. 1. As the NL is heated three distinct regimes are observed in the NL evolution. As the NL is heated it begins to decompose leading to a decrease in the optical reflectance signal but little change in the NL morphology as shown in the top row of images in Fig. 1. Upon heating the NL further, nanometer-sized GaN nuclei form as shown in images (c)-(e). Once formed, the nuclei grow in size as Ga atoms generated during the decomposition are transferred through the gas phase onto the growing nuclei, as shown in the second row of images (e)-(i). The nuclei reach a maximum size as shown in image (i) once all the original NL material has decomposed. Further annealing of the GaN nuclei leads to their decomposition and eventual disappearance as shown in the third row, images (j)-(m). The NL and GaN nuclei follow a similar decomposition mechanism and have a similar activation barrier of 2.7 eV, however, the more defective NL decomposes at a rate 6 times faster than the more crystalline GaN nuclei [6]. During the ramp to high temperature, the Ga source is turned back on to begin the high temperature growth on the nuclei, and this growth step is typically not controlled. Note that if the Ga is turned on too soon (image (d) in Fig. 1) or too late (image (l) in Fig. 1) the GaN nucleation density may either be too low or to high. Forming too many or too few GaN nuclei on the surface has been shown to lead to higher dislocation density films, so getting this growth step correct is crucial to achieving GaN films with lower dislocation densities.

Once the GaN nuclei are formed, the high temperature GaN growth is begun and the nuclei become larger sized grains. The standard two step growth process uses a GaN NL and one set of high temperature growth conditions, which results in rapid coalesce of the GaN nuclei and dislocation densities in the range from 1 to $5x10^9$ cm^{-2}. More recently, several groups, including us, have been using a three step growth process which uses a GaN NL and two sets of high temperature growth conditions [7]. Using this three step method, we have recently achieved dislocation densities as low as $4x10^8$ cm^{-2}. The key to the three step approach is reducing the temperature and NH_3 flow to produce pyramidal faceting as shown in Figs. 2(a) and 2(b), which bends the dislocations parallel to the surface as the GaN nuclei laterally coalesce [8]. The facet

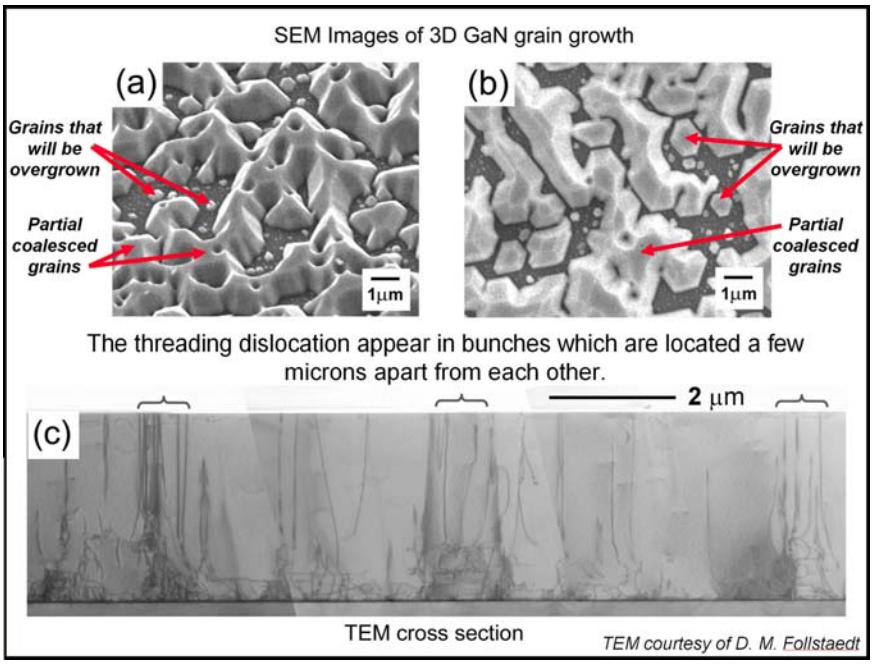

Fig. 2. SEM images after 15 minutes of GaN growth on top of an annealed NL from a (a) side view and (b) top view. The individual grains have started to coalesce and due to the reduced temperature and ammonia growth conditions have a pyramidal faceted morphology. Also shown in the image are smaller GaN grains that will eventually be overgrown once growth conditions are changed to favor lateral coalescence. As the larger grains overgrow the small grains dislocations are likely generated. Dislocations are also generated in bunches as the larger grains coalesce as shown in the TEM cross section shown in (c).

formation growth conditions have been studied extensively by Coltrin *et al.* [9, 10] and led to the choice of optimal growth conditions used for bending dislocations in our cantilever epitaxy work.

Images of the pyramidal growth stage after 15 minutes are shown in Figs. 2(a) and 2(b); as seen in the images some of the pyramidal faceted structures have begun to coalesce into larger GaN grains. Also shown in these two figures are smaller GaN grains between the larger structures that originate from additional nucleation on the sapphire once the high temperature growth is reinitiated. Because these smaller grains are closer to the sapphire surface, smaller fluxes of Ga and NH_3 reach them compared to the larger partially coalesced grains. Later in the growth as the lateral coalescence proceeds, the larger GaN grains must overgrow these smaller grains. During this overgrowth the larger grains intersect the smaller grains with the possible initiation of dislocations. Dislocations will also form as the larger grains coalesce to accommodate the lattice mismatch [11]. These dislocations are observed in Fig. 2(c) in bundles located 3-5 μm apart. Dislocation bending can also be observed close to the sapphire/GaN interface by the dislocations imaged parallel to the sapphire surface in Fig. 2(c).

2.2. Correlation between nucleation and dislocation density

Dislocation reduction can be achieved by reducing the number of GaN nuclei that initially form on the sapphire surface [12, 13]. Reports by Hashimoto *et al.* [12] and Moran *et al.* [13] demonstrate that lower nuclei density should decrease the dislocation density. This data is shown in Fig. 3 along with a geometric model to show how the dislocation density should scale with the nuclei density. If dislocations are assumed to be generated only during grain coalescence [11], then the nucleation density, n, will be related to the average spacing, L, of the nuclei by $n = 1/L^2$. At coalescence the grain diameter, d, will be equal to L such that $d = 1/n^{1/2}$. The dislocation tilt boundary, Γ, is $\sim mb/L$, where m is a constant and b is the relevant Burger's vector. The dislocation density, ρ, can be related to both the average spacing between grains, L, and the initial nucleation density, n, as shown in Fig. 3(a), resulting in the relationship that $\rho \propto n^{1/2}$.

In Fig. 3(b) results relating the dislocation density, ρ, to the nucleation density, n, from Hashimoto *et al.* [12] and Moran *et al.* [13] are shown. The short and long dashed lines are fits

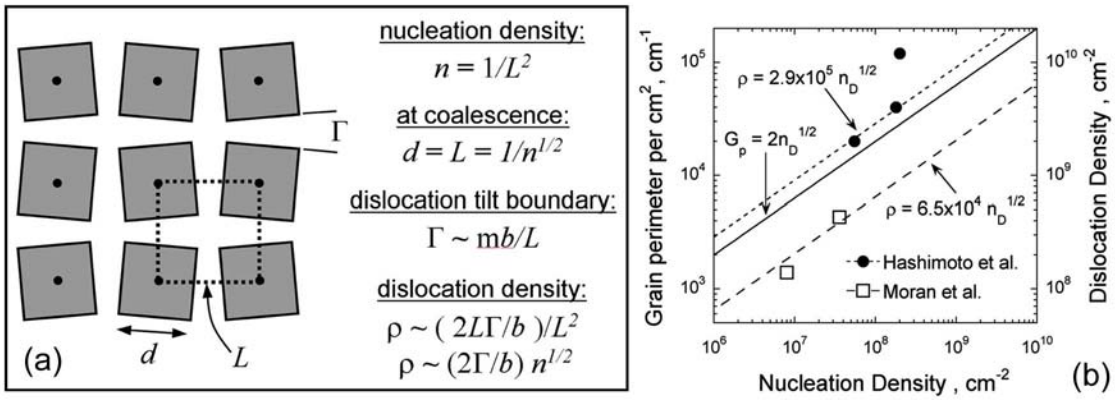

Fig. 3. (a). A geometric representation relating the nucleation density, n, to the resultant dislocation density, ρ, is shown. Once the analysis is completed, we find that $\rho \propto n^{1/2}$. The calculated grain perimeter per cm^2, G_p, (solid line) is plotted along the left axis vs. the nucleation density, n. The dislocation density, ρ, is plotted along the right axis vs. n for two experimental measurements from Hashimoto *et al.* (filled circles) [12] and Moran *et al.* (open squares) [13].The solid and dashed lines demonstrate the relationships $G_p \propto n^{1/2}$ and $\rho \propto n^{1/2}$, which fits the literature data well.

using $\rho = 2.9x10^5\ n^{1/2}$ and $\rho = 6.5x10^4\ n^{1/2}$, respectively. These fits suggest that dislocation density and nucleation density are correlated. (One data point from Hashimoto *et al.* [12] at the highest nucleation density and highest dislocation density is excluded from the fit because closer examination of the AFM images in Ref. [12] shows that the GaN nuclei are partly coalesced, resulting in an underestimation of the nucleation density.) The difference in the prefactors ($2.9x10^5$ vs. $6.5x10^4$) is due to the different substrates (sapphire vs. SiC) and growth pressures (150 torr vs. 760 torr) used for these growths. The differences in prefactors suggests that in addition to overall nucleation density the growth conditions also play an important role in dislocation reduction. Some of these factors may include preventing additional nucleation on the sapphire by increasing the growth pressure to induce higher GaN decomposition rates [6, 14] and increasing the smoothness of the starting substrate to produce grains with improved orientation. Using etched mesas and a SiC growth step, SiC surfaces were generated that contained either atomically smooth mesas with no steps or mesa with regular step arrays [15]. In the same growth run, GaN films on the atomically smooth mesas resulted in dislocation densities in the mid 10^7 cm^{-2} range, while GaN films on the regular step arrayed surface resulted in dislocation densities in the mid 10^8 cm^{-2} range [15]. This result stresses importance of substrate smoothness during GaN heteroepitaxy and that possible improvements to sapphire smoothness might result in GaN with reduced dislocation densities.

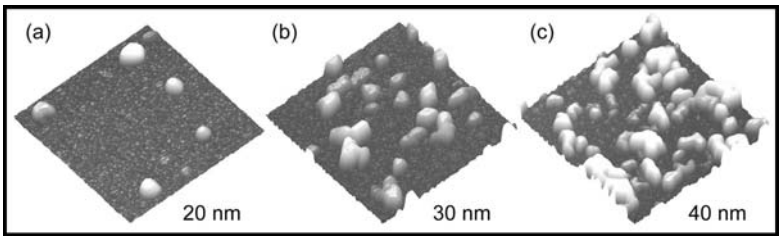

Fig. 4. AFM images of annealed GaN nucleation layers (NLs) with initial thicknesses of (a) 20 nm, (b) 30 nm, and (c) 40 nm. Each of these NLs were annealed until they reached a maximum degree of roughness as determined by the optical reflectance.

We have preliminary evidence to show that one simple way to control the nuclei density is by using starting nucleation layers with different initial thicknesses. This is shown in Fig. 4, where each of the NLs were grown to an initial thickness [16] and annealed to achieve the maximum roughness [5]. (Note that the annealed 40 nm thick NL has partly coalesced GaN nuclei

similar to the comment above for the Hashimoto et al. [12] data shown in Fig. 3(b)). Both the NL thickness and maximum roughness of the nuclei formation can be directly monitored using optical reflectance [5, 6] as well as the kinetic decomposition rates [16], allowing for increased control in the types of annealing schedules that can be used.

2.3. Using Optical Reflectance to Monitor GaN Growth

We (and many other groups) use optical reflectance to monitor all stages of GaN growth on sapphire. A typical reflectance curve is shown in red in Fig. 5 along with the temperature profile, which is shown in blue. Also shown in Fig. 5 are the various physical properties and changes to the GaN film morphology that can be measured using optical reflectance, which are shown in black, blue, and red lettering [6, 16, 17]. The film properties that are commonly measured by many researchers are shown in black, and include measurements of the NL thickness, the bulk growth rate, the 3D to 2D recovery time [17] and roughening [18]. For example, using reflectance we were able to control the NL thickness to within 29.81 ± 0.09 nm for 17 different NL growths. Our previous publication demonstrated how delaying the 3D to 2D recovery time reduced the dislocation density and lead to dramatic increase in near-UV LED output intensity [17]. More recently, we have used optical reflectance to measure the temperature dependent optical constants for sapphire, the GaN NL, and the bulk GaN film. In addition, we have developed methods to determine the decomposition rates by fitting the optical reflectance waveform [16].

We believe that fits of optical reflectance waveform using better models of the GaN morphology evolution should yield valuable information on the degree of NL roughness and potentially the initial nuclei density, as shown in red letters in Fig. 5. Using the reflectance waveform in this manner is very novel, and with further investigation of the GaN growth morphology, use of the reflectance waveform will change from “finger printing” the growth to quantitative guidance during the various growth modes. As part of this proposal we intend to determine the extent to

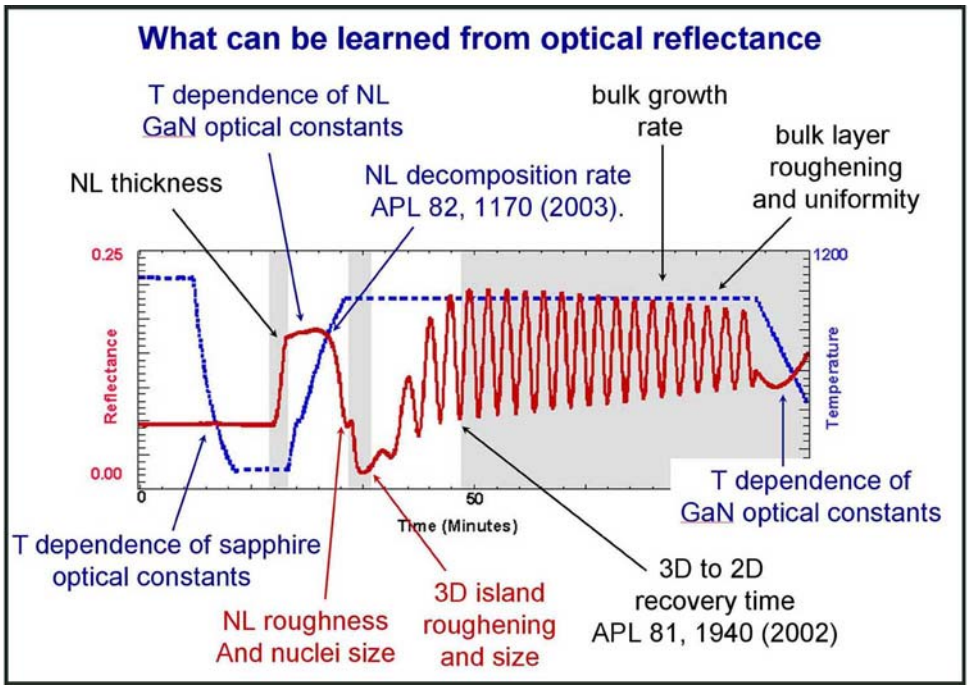

Fig. 5. In-situ optical reflectance (red) and temperature (blue) traces measured during MOCVD GaN growth. The optical reflectance provides a wealth of growth information, including well documented information (shown in black lettering) such as NL thickness and bulk growth rate, less well documented information (shown in blue lettering) such as NL decomposition rate and temperature dependence of the GaN and sapphire optical constants, and information that we hope to uncover in this proposal (shown in red lettering) such as the NL roughness, nuclei size and 3D island roughening characteristics.

which the reflectance waveform can be used in this manner (as described in Task description section). Our intent for this proposal is to fully model the entire reflectance waveform to obtain as much diagnostic information on the evolving film as possible. This will be a significant aspect of our proposal, because we believe that measuring the nanometer-scale nuclei density and size will ultimately prove critical to reducing the dislocation density.

3. Comparison of actual accomplishments to proposed goals

3.1. Overall Program Goals

1. Determine the correlation between nanoscale GaN nuclei density and resultant dislocation density in GaN full films.

2. Develop techniques to reduce the GaN nuclei density and subsequent dislocation density. These will include varying the GaN nucleation layer thickness and annealing schedules to produce lower nuclei densities. After the GaN grains are established, SiN auto masking will be used to prevent the formation of additional GaN nuclei and to minimize the interaction between the laterally coalescing GaN grains and the sapphire substrate.

3. Develop sapphire conditioning procedures to vary the sapphire smoothness, including high temperature annealing, nitridation, and in-situ SiN formation. This should improve the GaN nuclei orientation and decrease the degree of misfit that must be accommodated during coalescence.

4. Develop a full growth model to fit the optical reflectance waveforms. Good fits should yield useful information on the GaN NL evolution, the GaN nuclei formation, and the coalescence of the films. The model will be used as a further guide to optimizing material quality.

Task 1 -Establish correlation between nucleation density and GaN dislocation density	
Month 12 Milestone	Month 18 Milestone
1.1 Determine correlation between nuclei density and dislocation density in GaN films. **COMPLETED**	
Task 2 -Develop growth methods that limit the GaN nuclei density, preventing growth between nuclei.	
Month 12 Milestone	Month 18 Milestone
2.1 Develop controllable GaN nuclei densities from 10^6 cm^{-2} to 10^7 cm^{-2}. **COMPLETED**	2.2 Prevent additional GaN nuclei from forming during high temperature GaN growth; determine using AFM or SEM. **COMPLETED**
Task 3 - Condition sapphire substrates to improve GaN nuclei orientation.	
Month 12 Milestones	Month 18 Milestone
3.1 Decrease sapphire RMS roughness by a factor of 2, as measured by AFM. **COMPLETED**	3.2 Achieve GaN films on sapphire with dislocation densities of 10^8 cm^{-2}. **COMPLETED**
Task 4 - Develop full growth model to fit the optical reflectance waveforms during growth.	
Month 12 Milestones	Month 18 Milestone
	4.1 Develop model for GaN growth and corresponding optical reflectance waveform. **INITIATED** 4.2 Use two color optical reflectance to determine if nuclei density and roughness can be extracted. **NOT COMPLETED**

3.2. Program Milestones

The 12 month and 18 month program milestones are listed below. After each milestone is its status at the completion of the program. All milestones in Tasks 1 to 3 were met. The milestones in Task 4 were not met and were not instrumental to the completion of the primary milestone 3.2 which was to "achieve GaN films on sapphire with dislocation densities of 10^8 cm^{-2}".

3.3. Tasks to Meet Program Goals and Actual Accomplishments

Below are listed each of the four tasks developed for this program. Following each task is a paragraph on the actual accomplishments made in each task, along with a description of how the accomplishments listed difference from the program goals in the proposed work. Scientific details for each of the tasks are described in Section 4 in the Summary of Project Activities.

Task 1 – Establish correlation between nucleation density and GaN dislocation density.

The correlation between nucleation density and GaN dislocation density is a major assumption in this work and in several recent publications. While evidence has been presented in the literature for such a correlation [12, 13], typically only two or three data points have been used to infer the correlation. We hope to not only prove the correlation, but also demonstrate that it follows specific power law dependence as described in the previous section, namely $\rho \propto n^{1/2}$. For this task we will develop methods to vary the nuclei density, including multiple NL growth and annealing steps and different NL thicknesses and annealing schedules.

The nuclei density will be determined by quenching the growth conditions by lowering the temperature and switching to N_2 flows to freeze in the structure. During the cool down changes to the annealed nuclei structure can be monitored using reflectance, and ideally if no change occurs the reflectance signal should remain constant after the thermal component of the reflectance signal is account for. The nuclei distributions will then be determined using AFM and nuclei densities from partially coalesced nuclei will be estimated based on the extent of coalescence and average nuclei size.

Following the establishment of methods to grow different nuclei densities, full coalesced films will be grown using a standard high temperature growth procedure. For each of the nuclei densities developed in Task 1.1, fully coalesced GaN films will be grown on these layers. The dislocation densities on the full films will be determined using x-ray diffraction, as previously described in Ref. [19].

Task 1.1—Develop templates that have evolved nuclei densities ranging from 10^7 to 10^9 cm^{-2}.

Primarily, this will be accomplished by varying the nucleation layer (NL) thickness and other growth parameters to establish different GaN nuclei densities. As the NL is annealed, the sample will be quenched in temperature once the maximum roughness of the NL has been achieved (as determined by optical reflectance). We previously used a similar technique to study the GaN NL evolution [5]. By quenching the temperature in this way, the nuclei distributions will be captured in time and the nuclei density will then be determined using AFM. Nuclei densities from partially coalesced nuclei will be estimated.

Accomplishments and changes for Task 1.1 – This task was accomplished by recognizing that the nucleation density depended on the initial nucleation layer thickness. The initial nucleation thickness was measured using optical reflectance following Ref [5]. Nucleation density was estimated using AFM scans. In some of these scans the nuclei could be counted individually, while in other of the scans where the GaN nuclei had partly coalesced, we estimated the nucleation density based on a method described in more detail in Section 4.1. From this approach we were able to achieve nucleation densities exceeding 10^9 cm^{-2} to the low 10^7 cm^{-2}. Ultimately, when the multiple cycles of GaN NL growth and annealing were used nucleation densities well

below 10^7 cm^{-2} were achieved. No changes from the initial research plan were encountered in Task 1.1

Task 1.2—Determine the dislocation density in fully coalesced GaN films on templates with variable GaN nuclei densities.

For each of the nuclei densities developed in Task 1.1, fully coalesced GaN films will be grown on these layers. The dislocation densities on the full films will be determined using x-ray diffraction, as previously described in Ref. [19].

Accomplishments and changes for Task 1.2 – Once a range of nucleation densities had been achieved full GaN films were grown on these NLs and the dislocation densities were estimated using XRD. From initial studies there was only a weak correlation between the nucleation density, n_D, and the resultant dislocation density, ρ, was observed. Later once the correlation between the nucleation density and the NL thickness was experimentally verified, the dependence of the screw and edge component dislocation densities on the NL thickness and corresponding nucleation density were demonstrated. This is described in more detail in Section 4.1.

Task 2 – Develop methods that limit the GaN nuclei density, preventing growth between nuclei.

Growth conditions will be developed to further reduce the GaN nuclei density and subsequent dislocation density. These experiments will include varying the GaN NL thickness and annealing schedules to produce lower nuclei densities. One approach by Lang *et al.* [20] uses several NL growth and annealing cycles to achieve large and sparse (low density) nuclei. Another method will use changes to the NL annealing conditions including, less NH_3, higher pressure, and higher temperature to favor the growth of fewer, larger GaN nuclei

After the GaN grains are established, SiN auto masking will be used to prevent the formation of additional GaN nuclei and to minimize the interaction between the laterally coalescing GaN grains and the sapphire substrate. GaN growth at higher flow rates and higher pressures will also be investigated to determine if this can reduce additional nuclei formation. Our goal will be to control the GaN nuclei density in the range 10^6 to 10^7 cm^{-2}, as this should allow us to achieve dislocation densities in the low 10^8 cm^{-2} as shown in Fig. 3(b) by extrapolating the thick dashed line to this range of nuclei densities.

In addition to reducing the GaN nuclei, methods will be investigated to increase the lateral growth rate to increase the coalescence distance. If successful, additional decreases in the nuclei density can be used to further reduce the GaN dislocation density. To achieve faster lateral coalescence growth rates, we will investigate higher growth temperatures, higher reactor pressures, and higher flow rates.

Task 2.1—Vary growth conditions to limit GaN nuclei formation on sapphire

For this subtask, methods will be developed to limit GaN nuclei formation. These methods will include decreasing the thickness of the NL, using multiple NL layer growth and annealing schedules [16], and changing the NL annealing conditions (for example, less NH_3, higher pressure, higher temperature) to favor the growth of fewer, larger GaN nuclei.

Accomplishments in Task 2.1 – Methods were developed to limit the GaN nuclei formation, with the primary technique being using thin NLs. Multiple cycles of NL growth and annealing were also used to achieve the lowest nucleation densities as described in Section 4.2. The NL annealing conditions were only varied slightly. In one set of experiments the total flow through the reactor was varied, resulting in not much change in the overall nucleation density. Other annealing conditions were not necessary due to the achievement of nucleation densities of ~$4x10^6$ cm^{-2} using the multiple cycle NL growth and annealing technique. Using this method for reducing the nucleation density allowed us to achieve our ultimate milestone of dislocation densities < $1x10^8$ cm^{-2}.

Task 2.2—Develop auto-masking techniques to prevent additional nuclei formation once high temperature growth is commenced.

Once the GaN nuclei are established on the surface, it is desirable that no additional nuclei be formed once the pyramidal or lateral growth processes are initiated. To prevent formation of additional nuclei, we will explore slower GaN growth rates, and using SiN auto-masking and nitridation to passivate the sapphire surface. After the nuclei are established, in-situ SiN auto-masking will also be used to prevent additional nuclei from forming when the GaN growth is restarted. GaN growth at higher flow rates and higher pressures will also be investigated to determine if this can reduce additional nuclei formation.

Accomplishments in Task 2.2 – Auto masking techniques were developed using codeposition of the silane dopant and ammonia, forming SiN. SiN is known to prevent GaN deposition at high temperature resulting in reduced nucleation. This method was applied to GaN films that were fully coalesced as well as the annealed sapphire substrate. Without the SiN treatment on the annealed sapphire wafers, rough GaN films resulted, while when the SiN treatment was used, specular GaN films resulted. Higher flow rates and higher growth pressure were not used to achieve lower nucleation densities or to improve the films because the SiN treatment was deemed to provide the formation of too many additional GaN nuclei.

Task 2.3—Develop growth methods to increase the lateral growth rate during coalescence.

In addition to reducing the GaN nuclei, methods will be investigated to increase the lateral growth rate to increase the coalescence distance. If successful, additional decreases in the nuclei density can be used to further reduce the GaN dislocation density. To achieve faster lateral coalescence growth rates, we will investigate higher growth temperatures, higher reactor pressures, and higher flow rates.

Accomplishments in Task 2.3 – Growth methods to improve the lateral growth rates were not studied, since success was made in reducing the nucleation density and achieving coalesced films meeting the milestone of achieving dislocation densities < $1x10^{8}$ cm^{-2}. Ideally, higher lateral growth rates could be used to further decrease the dislocation densities, however, this may depend more on the reactor design that the actual growth conditions used. Clearly, more research needs to be conducted in reactor design to optimized group III nitride growth.

Task 3 – Condition sapphire substrates to improve GaN nuclei orientation.

We will develop sapphire conditioning procedures to vary the sapphire smoothness, including high temperature annealing, nitridation, and in-situ SiN formation. This should improve the GaN nuclei orientation and decrease the degree of misfit that must be accommodated by dislocation generation during coalescence.

Since ready-to-use sapphire surfaces still contain a substantially amount of surface polish damage, we will use high temperature annealing of sapphire in oxygen or air furnaces to anneal out this surface damage. If successful, we anticipate improvement in the crystallographic step structure and reduced RMS roughness in AFM images of these flatter sapphire surfaces.

Although reactant flows have been studied as growth parameter variables, few studies have examined changes to the initial sapphire surface when the sapphire is exposed to either ammonia (nitridation), high temperature H_2, or high temperature SiN film formation. We will explore the possible benefits of these surface treatments and quantify their influence on the GaN nuclei density formation.

Task 3.1—Oven annealing of sapphire in air or oxygen furnace.

Since ready-to-use sapphire surfaces still contain a substantially amount of surface polish damage, we will use high temperature annealing of sapphire in oxygen or air furnaces to anneal out this surface damage. If successful, we anticipate improvement in the crystallographic step structure and reduced RMS roughness in AFM images of these flatter sapphire surfaces.

Accomplishments in Task 3.1 – Sapphire was annealed in a tube furnace for up to 16 hours under a variety of annealing gas compositions. Ultimately the sapphire smoothness was improved by a factor of 2 meeting milestone 3.1. The annealing removes residual polishing damage and the sapphire steps are more clearly observable. Comparisons of the different annealing gas combinations are highlighted in Section 4.3 along with the final choice which provided the smoothest GaN films.

Task 3.2—Sapphire nitridation and SiN formation to smoothen the surface.

Although reactant flows have been studied as growth parameter variables, few studies have examined changes to the initial sapphire surface when the sapphire is exposed to either ammonia (nitridation), high temperature H_2, or high temperature SiN film formation. We will explore the possible benefits of these surface treatments and quantify their influence on the GaN nuclei density formation.

Accomplishments in Task 3.2 – For this task SiN treatment of the annealed sapphire wafers was critical to achieving specular GaN films. Exposure of the sapphire wafer prior to GaN growth at temperature below 900 °C was found to not be effective in changing the overall GaN growth.

Task 4 – Develop full growth model to fit the optical reflectance waveforms during growth.

Our team has extensive experience in developing models for growth and calculating how differences in these growth models affect the optical reflectance waveforms [5, 6, 16]. In this task, we will develop a full GaN growth model and use it to simulate reflectance waveforms for comparison to the experimentally measured waveforms. Ultimately we will use the model and quality of the fit to the optical reflectance waveform to obtain useful information on the GaN NL evolution, the GaN nuclei formation, and the coalescence of the films.

A reflectance waveform simulator will be developed accounting for all aspects of GaN growth, including sapphire annealing, GaN NL growth, GaN NL annealing and decomposition, GaN nuclei formation, initial growth on the GaN nuclei, roughening as the GaN nuclei grow, GaN grain coalescence and smoothing of the surface, and surface thickness non-uniformity.

Since the GaN nuclei have similar sizes but different number densities as they evolve, they should attenuate shorter wavelength light to a greater extent compared to longer wavelength light. This may potentially enable us to extract information on the nuclei density during growth.

Task 4.1—Develop model and reflectance waveform simulator to model GaN growth on sapphire

A reflectance waveform simulator will be developed accounting for all aspects of GaN growth, including sapphire annealing, GaN NL growth, GaN NL annealing and decomposition, GaN nuclei formation, initial growth on the GaN nuclei, roughening as the GaN nuclei grow, GaN grain coalescence and smoothing of the surface, and surface thickness non-uniformity.

Accomplishments in Task 4.1 – Methods were developed to model the nucleation formation and growth; however, full modeling of the GaN growth on these nuclei was not completed during this project. In the future the modeling may be extended to include full film growth simulations.

Task 4.2—Determine if multi-wavelength reflectance can be used to obtain information on GaN nuclei density.

Since the GaN nuclei have similar sizes but different number densities as they evolve, they should attenuate shorter wavelength light to a greater extent compared to longer wavelength light. This may potentially enable us to extract information on the nuclei density during growth.

Accomplishments in Task 4.2 – Unfortunately, no work was done on this task due to time constraints and the greater focus to achieve Milestone 3.2, "Achieving GaN films with dislocations densities < $1x10^8$ cm^{-2}".

4. Summary of project activities

4.1 Task 1 summary

Task 1 – Establish correlation between nucleation density and GaN dislocation density.

The major focus of Task 1 was to establish a correlation between nuclei density and dislocation density. Our goal is to determine the correlations between the nuclei density, *n*, and the GaN dislocation density, ρ. Depending on which scenario is assumed we expect either a power law dependence of $\rho \propto n^{1/2}$ or $\rho \propto n$. If dislocations are generated primarily during grain coalescence then the power law would be $\rho \propto n^{1/2}$. However, if the dislocations are generated randomly within the grains then the power law would be $\rho \propto n$. Irrespective of the actual power law dependence, we expect a decrease in the dislocation density if the nucleation density decreases.

In October of 2006, we began studies aimed at uncovering the possible correlation between nuclei density and dislocation density. For this study sample pairs were grown consecutively to achieve similar growth condition for separate measurement of nuclei and dislocation densities. The sample pairs consisted of (1) a grown NL that was annealed and the temperature quench so that the nuclei density can be determined using AFM ex situ, and of (2) an annealed NL identical conditions to the first run, but with a continued thick GaN layer for XRD determination of the dislocation density. To date, seven pairs of annealed nucleation layers (NLs) and thick GaN film have been grown. The GaN NLs were grown on sapphire, heated in flowing H_2, N_2, and NH_3 up to the high temperature growth condition of 1050 ^oC to develop the GaN nuclei. Once the GaN nuclei were developed the temperature was lowered to freeze the evolved nuclei structure. These annealed nucleation layers were imaged using AFM to measure the nuclei denisty.

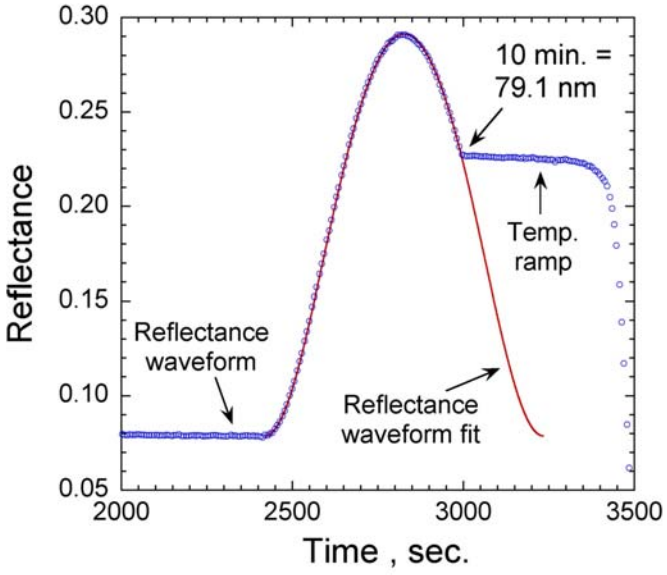

Fig. 6. The nucleation layer (NL) thickness can be determined from the measured reflectance waveform (shown in blue) by simulating the reflectance as the NL thickness increases (shown in red). From the measured and simulated reflectance waveform an NL thickness of 79.1 nm is estimated.

As a first attempt to control the nuclei density different GaN NL thicknesses were used. The NL thickness can be determined from the optical reflectance waveform as shown in Fig. 6 using the method described by Koleske *et al.* in J. Crystal Growth **279**, 37 (2005). As shown in Fig. 6, a measured reflectance waveform is plotted as open blue circles for a GaN NL grown for 10 minutes. To match the measured waveform, a simulated waveform is also plotted in Fig. 6 as a red solid line. The calculated waveform extends past the 10 minute NL growth time to simulate further evolution of the NL waveform. From comparison of the experimental (blue) and simulated (red) waveforms a NL thickness of 79.1 nm is estimated. In the present set of experiments, the NLs ranged in thickness from 12.95 to 79.1 nm which corresponded to GaN nuclei densities from ~$5x10^7$ cm^{-2} to greater than $1x10^8$ cm^{-2}.

AFM images of the annealed NLs where the initial nucleation thickness was varied are shown in Fig. 7. For these images the initial GaN NL thickness was varied from ~16 nm to ~79 nm,

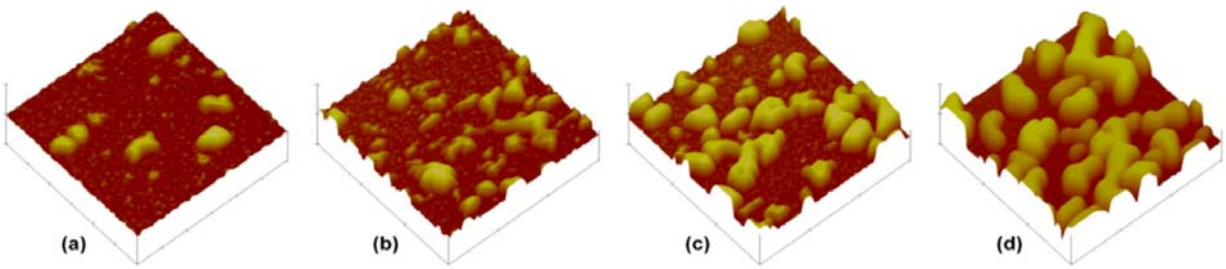

Fig. 7. Each of the nucleation layers (NLs) was grown for a) 2 min., b) 4 min., c) 6 min., and d) 10 min., which result in initial NL thicknesses of a) 15.9 nm, b) 33.5 nm, c) 51.4 nm and d) 79.1 nm, respectively. As the NL thickness increases the amount of material that is reincorporated into GaN nuclei increases along with an increase in the number of partly coalesced nuclei.

resulting in a planar GaN film across the surface. After the NL growth (Ga source is turned off) each of the layers is heated to 1050 ºC over 10 minutes under the same H_2, N_2 and NH_3 flow conditions and then the temperature is decreased and H_2 removed from the reactor. This freezes in the GaN nuclei structure observed in the AFM images. The GaN nuclei form from the decomposition of the NL as it is heated and the reincorporation of Ga atoms liberated during the decomposition recombine with NH_3 to form the nuclei. As shown in Fig. 7, as the NL thickness increases the amount of material converted into GaN nuclei also increases. Discrete GaN nuclei are clearly observed in Fig. 7(a), which is the thinnest NL, and little coalescence of the individual GaN nuclei is observed in larger scale images. However, as the NL thickness increases (in Figs. 1(b) to 1(d)) there is an increased tendency for the individual nuclei to coalesce. (Examples of coalesced and uncoalesced nuclei are shown in Fig. 3(c).) The biggest problem when the nuclei are partly coalesced is that it becomes difficult to get an accurate measure the nuclei density.

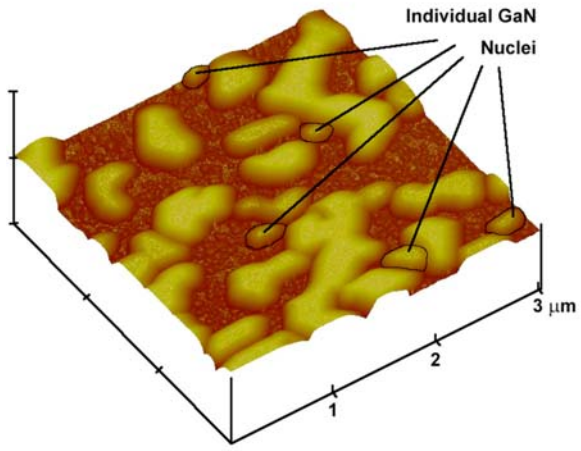

Fig. 8. A 3x3 μm size AFM image of an annealed NL with an initial thickness of 89.9 nm. Individual nuclei are circled that were used to determine the nuclei area.

Companion thick GaN films were grown using the seven different nucleation layer thicknesses. The dislocation density for these seven thick films was measured using the XRD method described by Lee *et al.* Appl. Phys. Lett. **86**, 241904 (2005). For these films we measured dislocation densities ranging from $8.4x10^7$ cm^{-2} to $2.4x10^8$ cm^{-2} for the screw component and 5.6 $x10^8$ cm^{-2} to $9.6x10^8$ cm^{-2} for the edge component. Over this limited range of nucleation layer thickness there was not a good correlation between the nuclei density and the dislocation density. Because the overall dislocation density is influenced by the NL growth, annealing conditions, and the high temperature growth conditions; several factors influence the resultant dislocation density even on films with higher nuclei density. For example, it is well known that a rougher NL produces a film with lower dislocation density.

Noting that it was difficult to obtain an accurate measure of the nucleation density for NLs that were partly coalesced, we developed a procedure to estimate the nucleation density in these partly coalesced nucleation layers. For this estimate we first measured the area of several smaller isolated nuclei as shown in Fig. 8. For the 3x3 μm AFM scan shown in Fig. 8, the NL was grown to an initial thickness of 79.9 nm. We assume that these smaller nuclei are not parts of larger

nuclei which make their individual areas easier to measure. For the AFM image shown in Fig. 8, the nuclei had an average size of 0.027 μm^2.

Once the area of the isolated nuclei was determined our next step was to calculate the area covered by all nuclei. For this measurement the Bearing measurement on the Nanoscope software was used as depicted in Fig. 9. The Bearing measurement provides a method of plotting and analyzing the distribution of surface height over a sample. In Fig. 9 the original AFM image is shown in the upper left. To measure the bearing area the threshold is total nuclei area the nucleation density was determined by dividing the total nuclei area by the individual nuclei area and normalizing by the area of the AFM scan, or $(5.261\ \mu m^2/0.027\ \mu m^2)/(3\ \mu m)^2 = 1.95x10^9\ cm^{-2}$. Averaging over several larger sized AFM scans gave a nucleation density of $2.7x10^9\ cm^{-2}$.

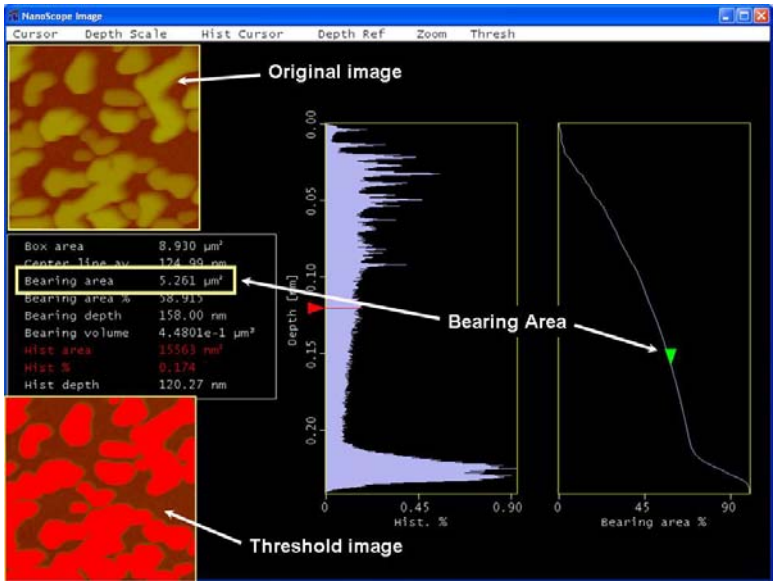

Fig. 9. Screen snapshot of the Nanoscope Bearing menu used to measure the total area of the annealed nucleation layer. After applying the threshold control, the bearing area slider (green arrow) can be moved until all of the nuclei are covered (red in threshold image) giving the total area of the nuclei covering the surface.

Another observation made early on in this program was the influence of the sapphire polishing on the nuclei formation is shown in Fig. 10. In Fig. 10(a), we show that the GaN nuclei can be imaged on the sapphire using Nomarski phase contrast microscopy. This capability to quickly image the GaN nuclei on sapphire will be an advantage later in this project for quick counting of GaN nuclei densities. Also in some regions of this image it appears that the GaN nuclei are clustered along lines on the sapphire surface. We believe that the GaN nuclei that form along these lines due to residual polishing damage on the sapphire. The clustering of the GaN nuclei along the scratch lines is shown in Figs. 10(b) and 10(c) which are 40x40 µm and 5x5 µm scan sizes. In Fig. 10(c), the increased nucleation density on the polishing scratches and increased coalescence is evident and is a problem for achieving

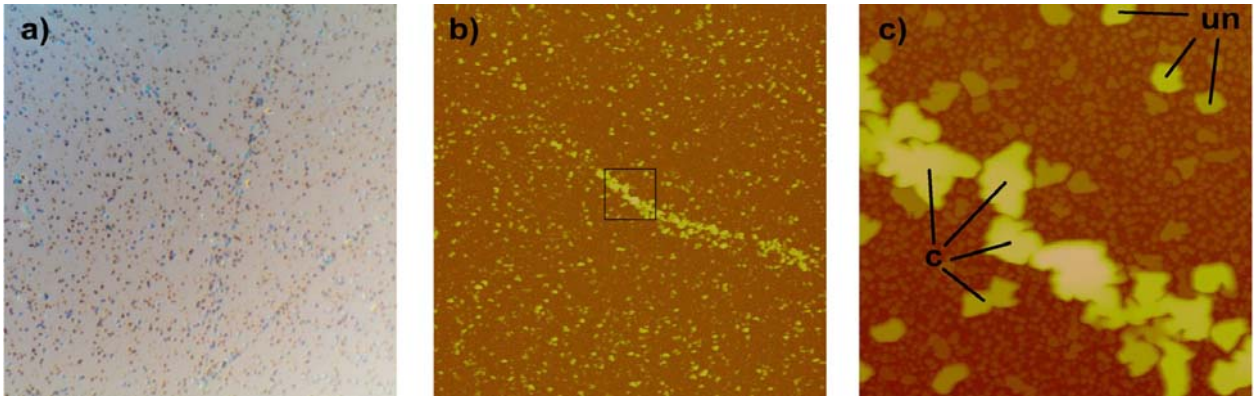

Fig. 10. Images of an annealed 15.9 nm thick GaN nucleation layer (NL). In a) is shown a Nomarski phase contrast image at a magnification of 150 x. Note that the GaN nuclei are visible and bunch together linearly, probably along polishing scratches on the sapphire. In b) and c) are AFM images of the annealed NL with images sizes of b) 40 µm x 40 µm and c) 5 µm x 5 µm. Image c) is an expanded image (black box) in the center of image b). In image c) are shown coalesced nuclei (denoted by c) where two or more nuclei have formed into a larger nuclei and uncoalesced nuclei (denoted by uc).

the uniform, low dislocation density substrates desired in this project. In previous GaN nuclei studies of GaN growth on SiC substrates, GaN nuclei were observed to form preferentially in concave defects such as the residual SiC polishing scratches. However as the polishing of the SiC substrates improved the uniformity of the GaN nucleation was improved resulting in GaN films with dislocation densities near $1x10^8$ cm^{-2}.

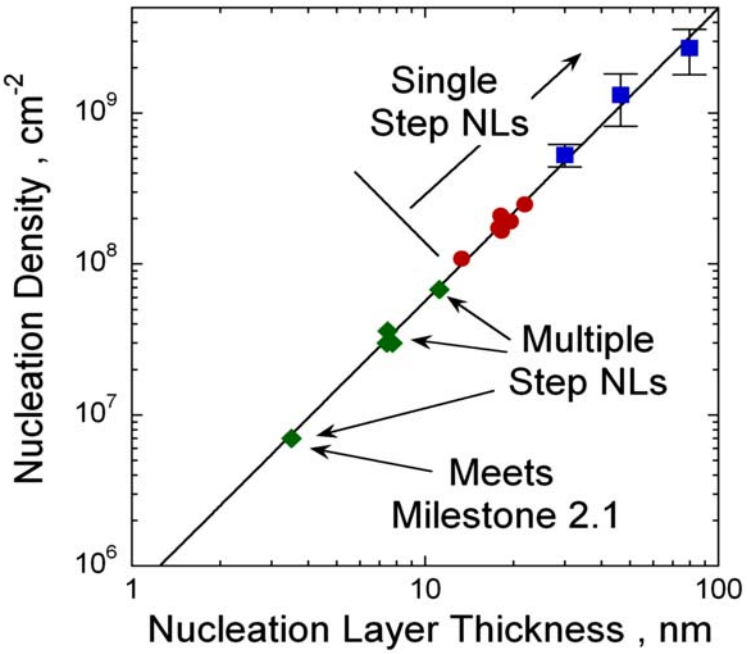

Fig. 11. The nucleation density is plotted vs. the initial nucleation layer (NL) thickness. The red circles are from single-step annealed nucleation layers (NLs). The green diamonds are from films with multiple cycles of NL growth and annealing. The blue squares are from estimates of the nucleation density obtained by measuring the total nucleation density divided by the nuclei area obtained from the smallest individual nuclei as described in the text.

Using methods developed in Section 4.2 where the nucleation density was reduced, we were able to establish a relationship between the nucleation layer thickness and the nucleation density. This relationship is plotted in Fig. 11, where the nucleation densities are plotted for single NL growth and anneals in red, single NL growth and anneal where the nucleation density had to be determined using the bearing method described above, and multi-NL growth and annealing described in Section 4.2 in green. For the multi-NL growth and annealing only the initial NL thickness is plotted in Fig. 11. The power law dependence relating the nucleation density, n_D to the nucleation layer thickness, d_{NL}, follows n_D = const. x d_{NL}^2. This is one of the major findings of this program that the nucleation layer thickness influences the resultant nucleation density is such a predictable way.

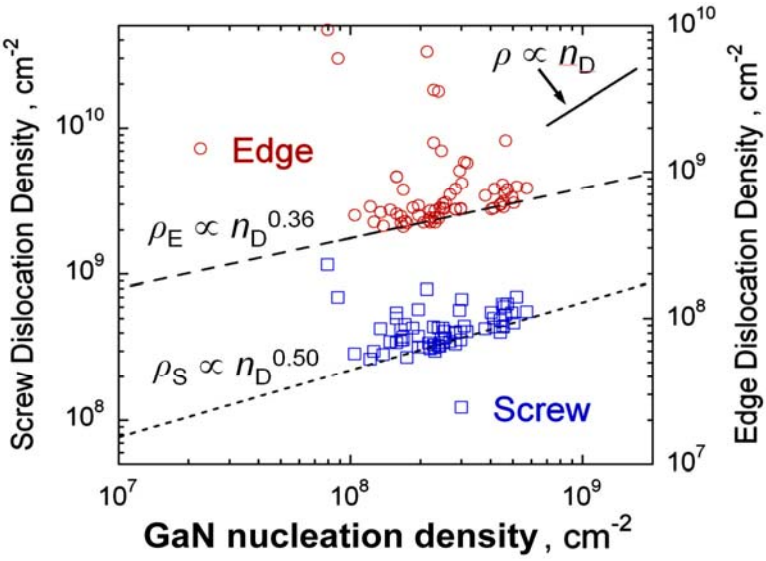

Fig. 12. For the edge component dislocation density, ρ_E is proportional to $n_D^{0.36}$, while for the screw component dislocation density, ρ_S is proportional to $n_D^{0.50}$. Also shown as the short solid line is the relationship, $\rho \propto n_D$, for comparison.

After another attempt to grow matched pairs of films to measure both nucleation density and dislocation density to establish a correlation between n_D and ρ, we decided as an exercise to use the relationship between n_D and d_{NL} to transform previously measured dislocation density data determined as a function of nucleation layer thickness. As shown in Fig. 12, the screw (open squares – left axis) and edge (filled circles – right axis) component dislocation densities are

shown as a function of the nucleation layer thickness. The solid and dashed lines show the minimum dislocation densities achieved for each value of the nucleation layer thickness. The dislocation densities from previous experimental data where the NL thickness was measured were re-plotted using the relationship established in Fig. 11, namely n_D = const. x d_{NL}^2,. In Fig. 3, the dashed lines are power law fits through the minimum dislocation densities at each nucleation density, n_D. For the edge component dislocation density, we find that ρ_E is proportional to $n_D^{0.36}$, while for the screw component dislocation density, ρ_S is proportional to $n_D^{0.50}$. For comparison the relationship, $\rho \propto n_D$, is also plotted as a short solid line. Note that both dislocation components the scaling is closer to $n_D^{1/2}$ than n_D^1, implying that dislocations are generated along tilt boundaries as the GaN grain coalesce rather than being generated in the individual GaN grains before coalescence.

4.2. Task 2 summary

Task 2 – Develop methods that limit the GaN nuclei density.

Using only a single nucleation layer we were only able to achieve nucleation densities of ~1x10^8 cm^{-2}. As shown in Fig. 3, we needed to achieve nucleation densities of at least 1x10^7 cm^{-2} or lower. To achieve lower nucleation densities we used multiple NL growth and annealing sequences as previously discussed by Lang *et al.* (phys. stat. sol. (a) 203, R76– R78 (2006)). The optical reflectance waveform showing four NL growth and annealing cycles is shown in Fig. 13. In the figure each cycle growth and annealing is denoted along with the thickness of the deposited NL material as measured from the change in the optical reflectance. As shown in Fig. 11 after two annealing cycles the reflectance signal approaches that of original sapphire surface, indicating substantial decomposition of the NL, while after the third and fourth cycles the reflectance signal increases indicating that significant material has been deposited. The initial NL thickness deposited in step 1 is thinner (7.6 nm) than previous NL growth and annealing sequences and after four cycles the total deposited NL material is 41.6 nm thick.

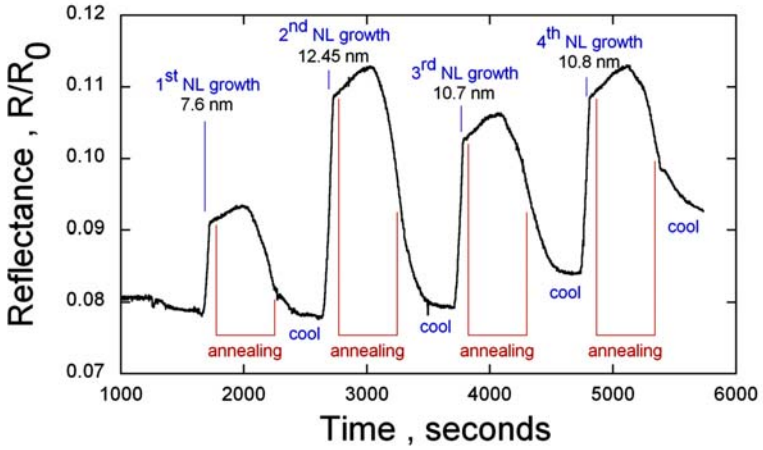

Fig. 13. Optical reflectance waveform plotted vs. time showing four nucleation layer (NL) growth and annealing cycles. Each of the NL growths and annealing cycles are depicted in the figure. Although the NLs were each grown for the same amount of time there is a different amount of NL material deposited during each cycle. The total thickness of the deposited NL material can be obtained from the change in optical reflectance.

Atomic force microscope (AFM) images (10 μm x 10 μm) are shown in Fig. 14 for annealed NLs demonstrating a wide range in nuclei densities. The AFM image of the four cycle NL discussed in the previous paragraph is shown in Fig. 12(a). For comparison single cycle NLs with initial NL thicknesses of 13.0 and 46.5 nm are shown in Fig. 12(b) and (c). In image (a) the reduced nuclei density is apparent and the nuclei are larger than the single cycle NLs in images (b) and (c). The reason the larger nuclei are larger in image (a) is because after the nuclei are formed in the first NL growth and annealing cycle NL material from the second through fourth steps is added only to these established nuclei and no new nuclei are formed. Even though approximately 40 nm of NL material is deposited in both images (a) and (c) the nuclei density

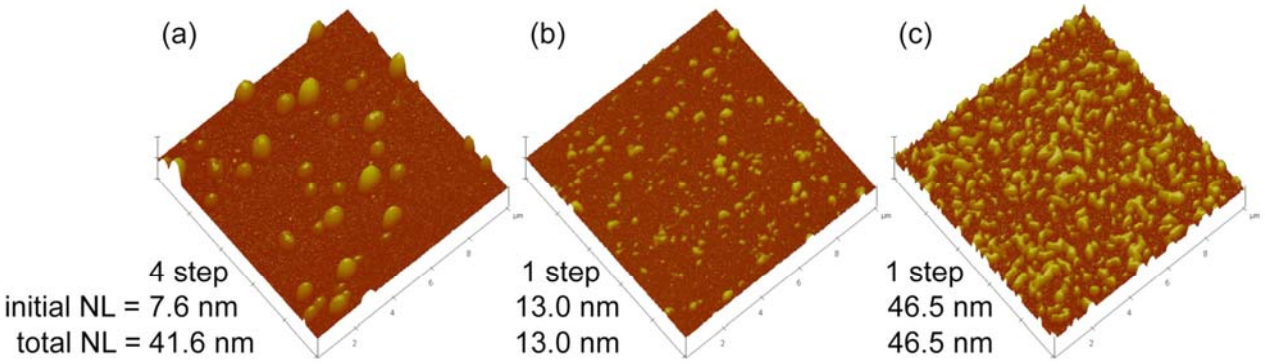

Fig. 14. Atomic Force Microscope (AFM) images (10 μm x 10 μm) of annealed nucleation layers (NLs) showing the range of nucleation densities that can be achieved. For each of the images the initial NL thickness is shown along with the total NL thickness as measured using optical reflectance. Note that the fewest number of nuclei (~$3.0x10^7$ cm^{-2}) is achieved in image (a) which has a total NL thickness (after four NL deposition and annealing cycles) similar to the thickness in image (c). Also note that the nuclei size is substantially larger in image (a) compared to images (b) and (c).

and size can be substantially changed using multiple growth and annealing cycles. Using this multi-step NL growth and annealing we believed that we could achieve nucleation densities less than 10^7 cm^{-2} using initial NL thicknesses < 4 nm would allow us to accomplish Milestone 2.1: Develop controllable GaN nuclei densities from 10^6 cm^{-2} to 10^7 cm^{-2} as shown in Fig. 11.

Auto masking techniques were developed to limit GaN nucleation on the sapphire. The development of this auto masking played a large role in the dislocation reduction on the annealed sapphire wafers described in Section 4.3.

To determine the extent of Silicon nitride (SiN) formation necessary to limit GaN growth, several growth conditions were varied to improve the SiN uniformity. These growth conditions included lower growth pressure and temperature. The best growth conditions established are at a

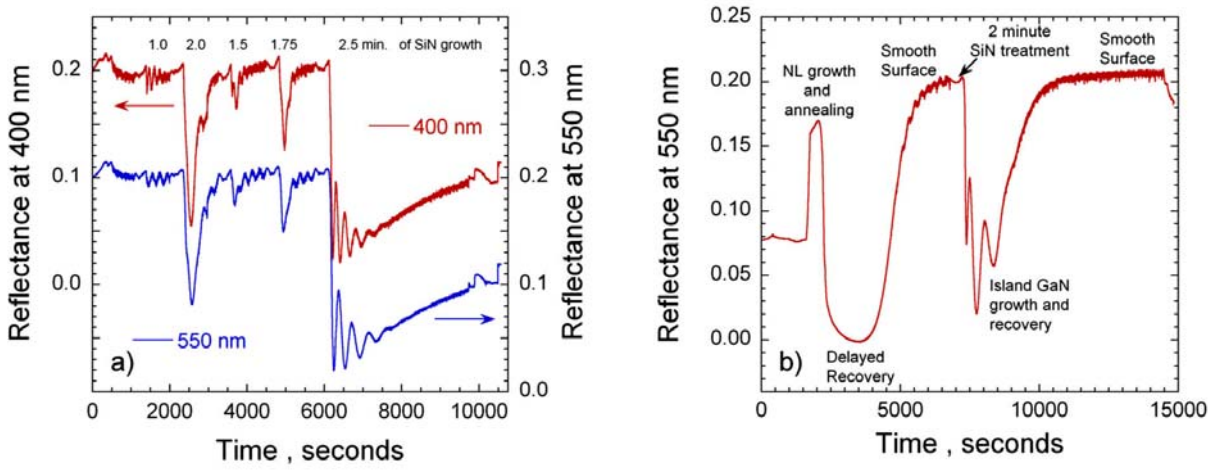

Fig. 15. Optical reflectance waveforms showing (a) different timed SiN treatments of the GaN surface and (b) a standard GaN template growth run on sapphire with a 2.0 minute SiN treatment half way through the growth run. In (a) SiN growth times ranged from 1.0 to 2.5 minutes. For each case (except the 2.5 minute treatment) the GaN film eventually recovery to a specular film, however for the 2.5 minute treatment of the film showed gradual recovery of the GaN film but was ended before complete recovery was attained. In (b) a full GaN growth run was conducted and once the film was full coalesced (smooth surface in image) the GaN surface was exposed to a 2 minute SiN treatment followed by continued GaN growth.

pressure of 70 torr, a temperature of 900 °C, a silane flow rate of 5.3 nanomoles/min., and a standard NH_3 flow rate typically used for GaN growth of 7 SLM.

To determine the optimal thickness, the SiN growth times were varied from 1 to 2.5 minutes and the optical reflectance waveform for this set of times is shown in Fig. 15(a). As the SiN growth time increased so did the reflectance attenuation and the time required to recover smooth GaN. The last exposure was 2.5 minutes which resulted in the largest reflectance attenuation and after ~ 1 hour of continued GaN growth the film was far from coalescence. After stopping this growth run, Nomarski images showed discrete partly coalesced grains that were widely separated. Also fewer small GaN grains were observed between the larger GaN grains, showing the feasibility of using SiN coatings to prevent additional nucleation after formation of the initial GaN nuclei.

As a further test of the SiN coating of GaN and growth recovery, a 2 minute SiN treatment was grown on a standard GaN template run as shown by the reflectance waveform shown in Fig. 15(b). After the SiN growth, the temperature was increased to 1060 ºC and GaN growth restarted, which produced a decrease in the reflectance signal due to the increased surface roughness from the GaN grain formation on the SiN coating. After ~ 1 hour the film recovers, resulting in a 15% reduction in the edge component dislocation density as measured by XRD compared to films with the same starting nucleation layer thickness. Further evaluation of this growth technique to limit the nucleation density and reduce the dislocation density is described in Section 4.3.

4.3 Task 3 summary

Task 3 – Condition sapphire substrates to improve GaN nuclei orientation.

Sapphire conditioning procedures were developed to improve the sapphire smoothness. This this was accomplished by using high temperature oven annealing of the sapphire. Improving the sapphire smoothness should improve the GaN nuclei orientation and decrease the degree of misfit that must be accommodated by dislocation generation during coalescence. In addition, as received sapphire surfaces still contain a substantial degree of surface polish damage and removing this damage may be critical for better GaN grain orientation. If successful, we anticipate improvement in the sapphire crystallographic step structure and reduced RMS roughness as measured by AFM images of these flatter sapphire surfaces.

An AFM image for an as received sapphire wafer is shown in Fig. 16(a). Typically, the sapphire wafers have a good overall RMS roughness of less than 0.1 nm, however the surface morphology shows visible polishing scratches as shown by the arrows aligned to the scratch directions. Also, on the as received sapphire there is no well defined terrace and step structure although there is some hint of the terrace structure underlying the polishing damage to accommodate the 0.2º off-cut from the c-axis.

In an attempt to improve the sapphire surface morphology, we have annealed a sapphire wafer in an oxygen/argon atmosphere in a high temperature furnace. After annealing no polishing scratches are observed along with a much cleaner step and terrace structure. The steps appear regularly spaced due to the 0.2° off-cut. Removal of the polishing scratches and the appearance of a better defined terrace and step morphology suggest that some material has been removed or redistributed during the annealing. However the extent of this material redistribution is limited since the annealing temperature is only slightly greater than half of the sapphire melting temperature of 2040 °C, which results in wavy and patchy step edges. Later higher annealing temperatures for longer times were used to improve the step terrace structure.

Later a third annealing process was developed to improve the sapphire smoothness. Previously, we reported on a N_2 annealing process at 1200 ºC. The new process involves annealing the sapphire wafers to 1250 ºC in argon with a small amount of water. The surface morphology of

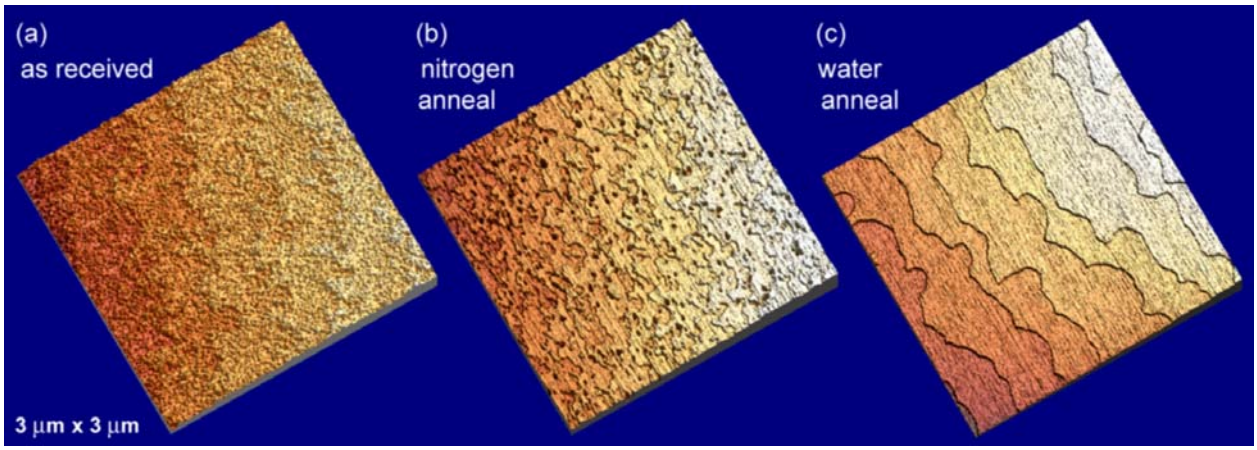

Fig. 16. Processed 3 μm x 3 μm AFM images of (a) as received polished 0.0º oriented sapphire, (b) sapphire that was annealed in nitrogen for 2 hours at 1200 °C, and (c) sapphire that was annealed in a dilute H_2O and argon for 4 hours at 1250 ºC. As previously mentioned in the August monthly report, the as received wafers do not have any clear discernable terrace and step structure. For the nitrogen annealed wafer, a clearer step and terrace structure is observed, however the step edges are not monotonically inclined. For the water annealed wafer the step edge are monotonically inclined and clearly defined.

three sapphire wafers is shown in Fig. 16. The three wafers are (a) an as-received sapphire wafer, (b) a sapphire wafer that was annealed in N_2 for 2 hours, and (c) a sapphire wafer that was annealed in argon with H_2O for 4 hours. Comparing the sapphire wafer morphology, the as-received wafers obviously do not have a discernable step structure, while both of the annealed wafers have observable step edges. Even though the as-received wafers do not have a clear step structure, over time we have developed our standard GaN growth process on them and can achieve dislocation densities as low as $4x10^8$ cm^{-2}. For the N_2 annealed wafers, steps edges are better defined and numerous single step height pits are observed embedded within the terraces. The most extreme change to the sapphire morphology occurred during the H_2O anneal which results in large terrace widths separated by monotonically inclined steps. Occasionally, pits were observed on the H_2O annealed sapphire (not shown in Fig. 16(c)), but were determined to not be detrimental to GaN growth.

Table I: RMS roughness in Angstroms

Image size	(a) As received	(b) N_2 annealed	(c) H_2O annealed	(a) / (c)
10 μm x 10 μm	0.89	1.08	1.09	0.81
5 μm x 5 μm	1.04	1.20	0.75	1.39
3 μm x 3 μm	1.11	1.25	0.65	1.71
0.5 μm x 0.5 μm	0.85	1.11	-	-
Terrace	0.85†	-	0.21	4.05*
1 step edge	0.85†	-	0.48	1.77
2 step edges	0.85†	-	0.85	1.00

† Used 0.5 μm x 0.5 μm for RMS roughness calculation used in last column.
*exceeds Milestone 3.1: Decrease sapphire RMS roughness by a factor of 2, as measured by AFM.

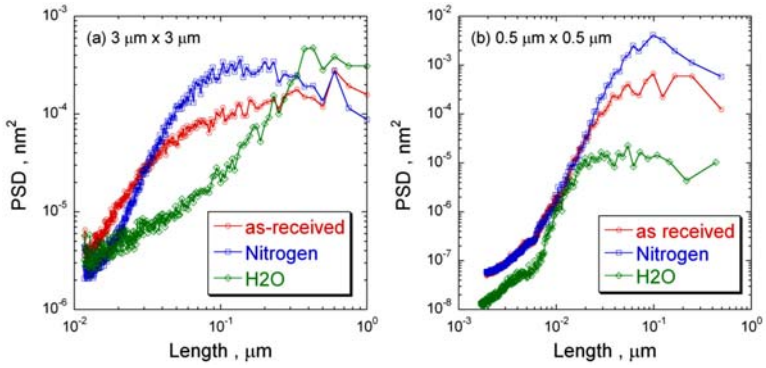

Fig. 17. Power spectral density (PSD) plots vs. length for each of the three samples shown in Fig. 1. In (a) the PSD was calculated for the entire 3 μm x 3 μm image, while in (b) a 0.5 μm x 0.5 μm image was calculated. For the H_2O annealed PSD shown in (b) the size was selected such that only the terrace was imaged resulting in a lower PSD at larger lengths.

The calculated RMS roughness for the as-received and two annealed sapphire wafers are shown in Table I. The RMS roughness is reported for different sized images and different regions on the H_2O annealed wafer. Additional RMS measurements for the H_2O annealed wafer were taken from images containing a terrace containing no steps, at terrace containing one step, and a terrace containing two steps. From the data in Table I, the N_2 annealed sapphire is slightly rougher than the as-received sapphire, while the H_2O annealed sapphire is substantially smoother at small length scales compared to the as-received sapphire, however the roughness increases as the scan size increases. Comparing the RMS roughness of the 0.5 μm x 0.5 μm images, the image containing the single terrace on the H_2O annealed sapphire has a roughness that is 4 times lower compared to the as-received sapphire. Including either one or two steps in the AFM image increases the roughness of the H_2O annealed sapphire images to the point where it is almost equal to the as-received sapphire. Even though the steps edges are well defined in Fig. 16(c) and the surface morphology appears more crystalline, the presence of step edges increases the RMS roughness substantially, making the reduction in surface roughness difficult as the length scale increases.

The difficulty of reducing the surface roughness at longer length scales can be observed in the power spectral density (PSD) plots shown in Fig. 17. The PSD plots for the as-received (red), N_2 annealed (blue), and H_2O annealed (green) for a 3 μm x 3 μm size scan are shown in Fig. 17(a) and a 0.5 μm x 0.5 μm size scan are shown in Fig. 17(b). The PSD plots are useful because they show what happens to the roughness as a function of length, l. Also the RMS roughness, σ, is typically calculated from the PSD by the formula, $\sigma = (\Sigma(\mathrm{PSD}(l))^{1/2}$. As shown in Fig. 17(a), the PSDs for the H_2O and N_2 annealed sapphire are lower than the as-received sapphire at small l, however, both increase for larger l. Near l = 0.1 μm for the N_2 annealed sapphire and near l = 0.4 μm for the H_2O annealed sapphire, the PSD becomes larger than the PSD for the as-received sapphire. Similar trends for each of the sapphire surfaces are also observed in Fig. 17(b). In Fig. 17(b), the PSD calculated for the H_2O annealed sapphire levels off for larger l, because the image used for the PSD shown contained a terrace with no steps.

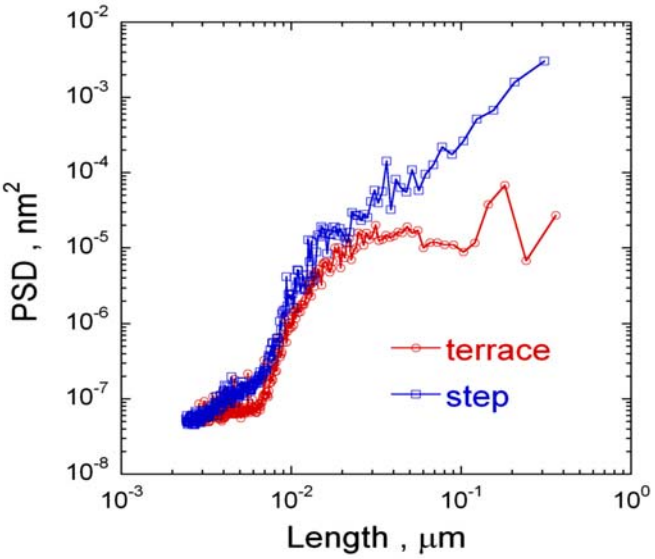

Fig. 18. Power spectral density (PSD) plots vs. length for the H_2O annealed wafer for terrace area containing no steps (red) and an area containing two steps running across the image (blue). Note that the presence of steps increases the PSD values at larger length scales.

The change in the PSD due to steps is shown in Fig. 18 for select regions of the H_2O annealed sapphire. For this figure, the PSD was calculated for an image with a single terrace (no steps) and an image containing several steps. Note that the PSD is larger at larger *l* for the image that contained several steps. What this PSD plot implies is that no matter how smooth the terraces are the step edges always increase the roughness at larger *l*. *Therefore we can not achieve milestone 3.1 unless we exclude step edges from the RMS roughness measurement.*

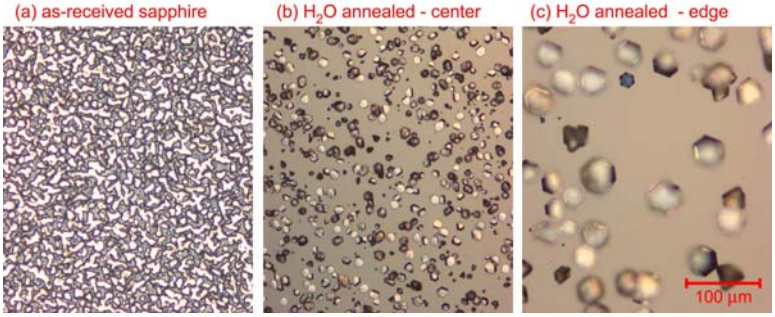

Fig. 19. Nomarski phase contrast images showing GaN growth (without a GaN nucleation layer) at 1050 ºC for (a) as-received sapphire, and (b) the H_2O annealed sapphire at the wafer center and (c) the H_2O annealed sapphire at the wafer edge.

After achieving the smoother terrace sapphire shown in Fig. 16(c), we initiated high temperature GaN growth to determine the nucleation characteristics of the H_2O annealed sapphire. Images after 1.75 hours of high temperature GaN growth are compared in Fig. 4 for the (a) as-received and (b) H_2O annealed sapphire. As shown in Fig. 19(a) the as-received sapphire produced a high degree of GaN nucleation and growth, leading to partial coalescence of some of the GaN grains. However, in Fig. 19(b) there was a decrease in the overall GaN nucleation and discrete GaN grains are observed. In Fig. 19(c) the edge of the H_2O annealed sapphire is shown and even fewer GaN grain are observed compared to the center of the wafer. This result suggests that the increased terrace smoothness on the H_2O annealed sapphire may be decreasing the overall nucleation rate.

Further confirmation of the decreased nucleation density on the H_2O annealed sapphire was observed when a standard two-step growth process was used to grow GaN films on the three sapphire surfaces shown in Fig. 16. The standard two-step GaN growth process consists of a 20 nm GaN nucleation layer deposited at 530 °C followed by high temperature GaN growth at 1050 °C. The optical reflectance waveforms for each of the three wafers are shown in Fig. 20. The reflectance waveform for growth on the as-received sapphire wafer looks similar to previous waveforms for this growth process. The reflectance waveform for the growth on the N_2 annealed sapphire wafer shows an increased degree of nucleation and more rapid coalescence which might be due to the slightly increased sapphire roughness compared to the as-received sapphire roughness (for roughness values see Table I). On the other hand, the reflectance waveform for the H_2O annealed sapphire shows less nucleation and no coalescence as observed by the reduced GaN nucleation layer thickness and the continuously

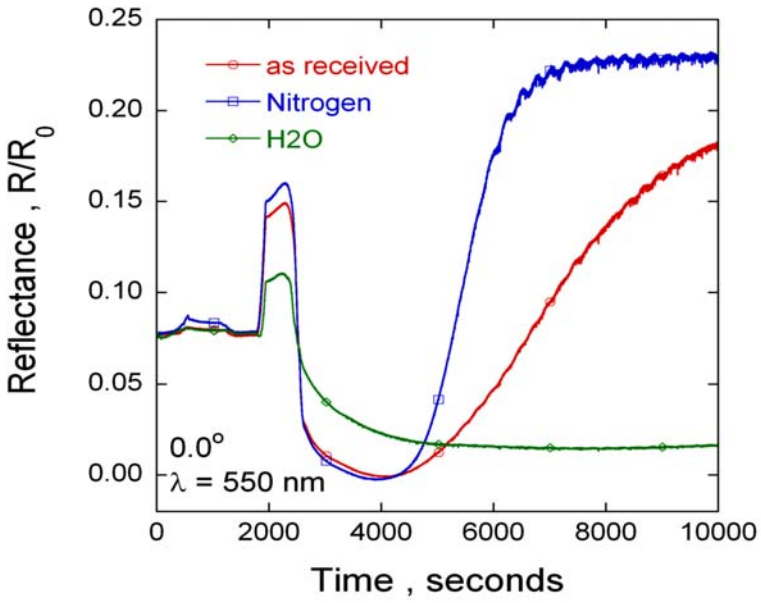

Fig. 20. Reflectance waveforms measured for GaN growth using standard "delayed-recovery" growth conditions for the three sapphire surfaces shown in Fig. 16.

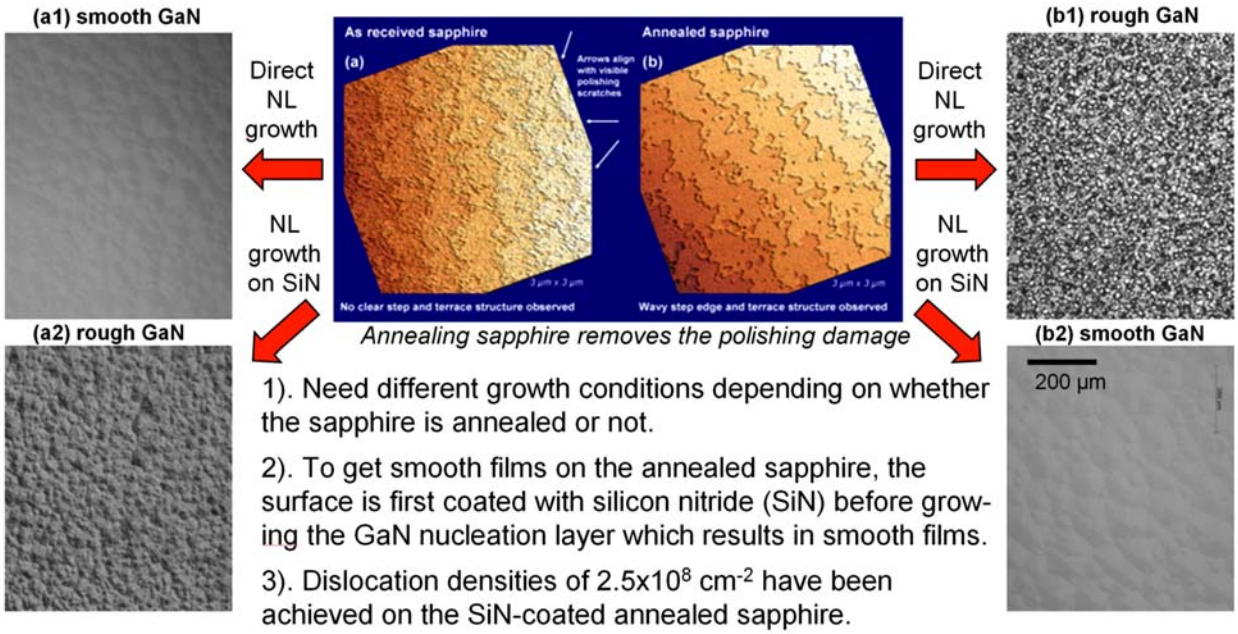

Fig. 21. GaN film morphology is shown to depend on the sapphire annealing and deposition of a thin silicon nitride layer prior to the GaN nucleation layer growth. In the center of the figure are shown AFM images of an as-received sapphire wafer and the same sapphire wafer after annealing. The main impact of annealing the sapphire is to remove surface polishing damage and to increase the presence of smooth step edges. Growth of GaN on the as-received sapphire wafer using the standard two step GaN growth process results in a smooth film as shown in image (a1), while the same growth process on the annealed sapphire wafer results in a rough film as shown in image (b1). On the other hand, if both sapphire surfaces are coated with a thin layer of silicon nitride before the two step growth process, GaN growth on the as-received sapphire results in a rough film as shown in image (a2), while GaN growth on the annealed sapphire results in a smooth film as shown in image (b2).

decreasing reflectance. The decreased nucleation on the H_2O annealed sapphire is likely due to the decreased sapphire roughness at smaller *l* compared to the as-received sapphire.

Our next goal was to achieve fully coalesced GaN films on the H_2O annealed sapphire. To accomplish this, different nucleation layer growth conditions were studied.

First, AlN nucleation layers were used at growth temperatures of 1100 and 1140 °C. These growth conditions are typically used to achieve GaN growth on SiC. For both of the AlN nucleation layers no continuous GaN film was formed on either sapphire wafer so the AlN nucleation layers were not pursued further for this research.

Next, GaN nucleation layers were used at growth temperatures of 500, 530, 600, and 900 °C, resulting in some specular films on the as received sapphire wafers and no specular films on the annealed sapphire wafers. For the GaN films grown on the as received wafers, the specular vs. non-specular results listed in Table 1 were somewhat expected based on prior experience and results in the literature. However, none of the GaN nucleation layer growth temperatures yielded specular GaN films on the annealed sapphire wafers. We speculate that the surface chemistry of the annealed sapphire wafers had been changed during the annealing process so that neither AlN or GaN nucleation processes could be used.

Finally, specular GaN films were achieved on the annealed sapphire wafers when a thin silicon nitride film was deposited at 900 °C before the growth of a low temperature GaN nucleation layer. Images of the sapphire with and without annealing and GaN morphology with and without

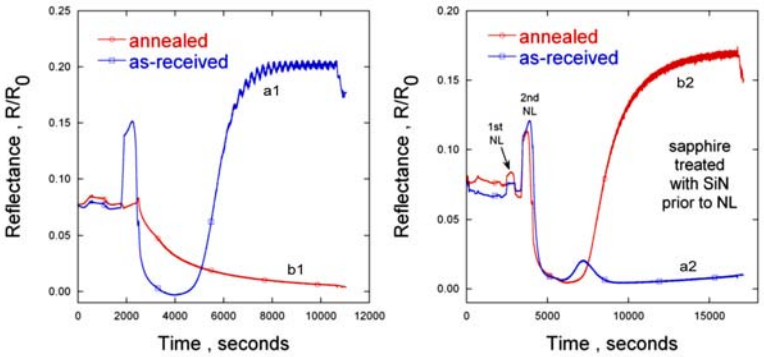

Fig. 22. Optical reflectance waveforms corresponding to the images (a1, a2, b1, and b2) from Fig. 1. Note that waveforms a1 and b2 recover after initial roughening (R/R_0 approaches zero), while waveforms a2 and b1 remain rough and have a near zero reflectance. Two cycles of the GaN nucleation layer growth and annealing were used for the GaN films on the silicon nitride treated sapphire wafers.

silicon nitride treatment are summarized in Fig. 21. In the center of Fig. 21 are AFM images of an as-received sapphire wafer and a sapphire wafer after annealing. As shown in the AFM image, by annealing the sapphire most of the surface polishing damage is removed and there is an increase in the presence of smooth step edges. The two different sapphire morphologies dramatically influence the GaN growth morphology as shown by images (a1, a2, b1, and b2). When using the standard two step growth process (i.e. low temperature NL followed by high temperature GaN), the GaN morphology is smooth on the as-received sapphire (image a1), and rough on the annealed sapphire (image b1). The rough and smooth GaN morphology can be reversed if a thin silicon nitride layer is placed on the sapphire before the growth of the low temperature GaN NL. With the silicon nitride layer the GaN grows rough on the as-received sapphire (image a2), while the GaN grows smooth on the annealed sapphire (image b2). For the films shown in images (a2) and (b2) a two cycle NL growth and anneal was used to reduce the nucleation density as described in previous reports.

For each of the GaN film images shown in Fig. 21 the corresponding optical reflectance waveform is shown in Fig. 22. Note that the surfaces of films (a1) and (b2) become smooth after initial roughening (region where the reflectance, R/R_0, reaches almost zero). However, the waveforms for films (a2) and (b1) roughen but do not recover.

To investigate the difference between the GaN nucleation layer evolution with and without SiN treatment, the GaN morphology evolution was studied by stopping the growth at different points and lowering the growth temperature to capture the structure. For the first experiment, the

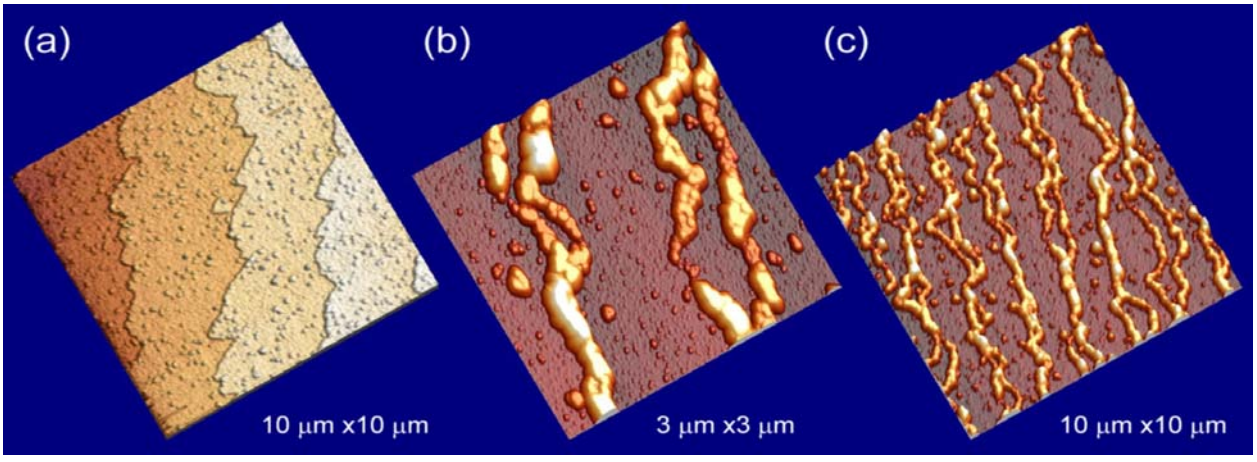

Fig. 23. AFM images of sapphire surface after annealing both before and after the growth of annealed GaN nucleation layers. The AFM image of the annealed sapphire surface is shown in image (a) and has monatomic steps with a jagged step-edge. This image also shows numerous sapphire islands on the terrace structure which produces a rougher surface. The morphology of the annealed GaN nucleation layers (NLs) are shown in images (b) and (c). For the annealed NLs a two step NL growth and annealing sequence was used. From these images it appears that the annealed NL material accumulates along the sapphire step-edges and islands on the terrace.

annealed sapphire wafer was heated in H_2 for 10 minutes at 1060 °C, followed by a 4.5 minute silicon nitride coating at 900 °C and then a two cycle GaN nucleation layer (NL) growth and anneal. After the second NL anneal the wafer was cooled in NH_3 and N_2 to prevent further morphology changes and "freeze in" the structure. As shown in Fig. 23(b) the GaN nuclei coalesce along the step edges when the annealed sapphire surface is is first treated using SiN. In Fig. 23(a) an AFM image of the annealed sapphire surface shows monatomic step heights with somewhat jagged step edges. Comparison of the film structure in Fig. 23(a) to the film structure in Fig. 23(b) shows that the nuclei form along the step edge. High temperature growth on these partly coalesced GaN nuclei resulted in sparsely-nucleated 1-2 micron sized GaN grains. *This reduced small-scale nucleation is evidence that nucleation can be limited to only those nuclei which become large GaN grains in the fully coalesced film, which is the goal of Milestone 2.2.*

During the heterogeneous nucleation of the GaN on the annealed sapphire surface, we expect the GaN to preferentially nucleate at kink or step-edge sites, especially after the silicon nitride coating presumably reduces nucleation on the sapphire terraces. This is precisely what is observed in the AFM images of the annealed GaN nucleation layer shown in Figs. 23(b) and 23(c), where the connected-strand nuclei coalesce along step edges and the isolated nuclei coalesce near the edge of the raised sapphire islands. The major reason for nucleating along step edges is to improve the GaN grain orientation.

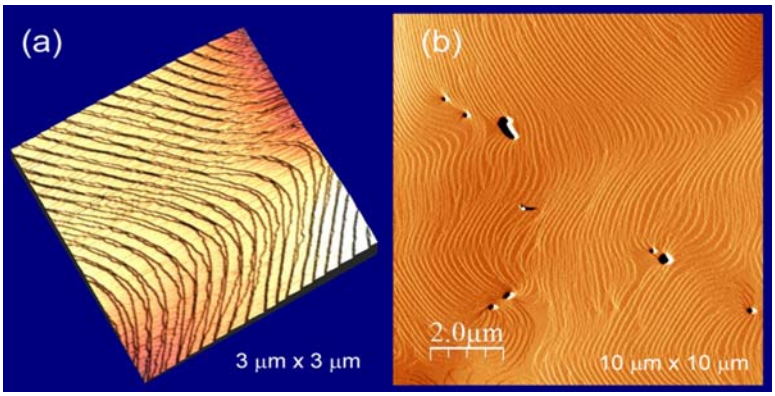

Fig. 24. AFM images of the coalesced GaN film grown on the SiN treated annealed sapphire. In image (a) is shown the well developed GaN step structure with alternating A and B step edges. A derivative AFM image is shown in image (b) which more clearly shows the step structure over a 10 μm x 10 μm region. Note that there are several large pits due either to incompletely coalesced GaN grains or dislocations.

Finally, regions where the GaN films did coalesce after the three hour high temperature growth are shown in Fig. 24. In these AFM images, a well developed GaN step structure is observed with alternating A and B type step-edges. This step structure is reminiscent of the step structure observed over the defect-free regions of epitaxial lateral overgrowth (ELOG) grown GaN. In Fig. 24(b) the derivative AFM image is shown which illustrates the step structure over a larger 10 μm x 10 μm region. Note that there are several large pits due either to incompletely coalesced GaN grains or to dislocation cores. These images look promising that this growth procedure will allow us to achieve our milestone of producing GaN with dislocation density of $1x10^8$ cm^{-2}.

One issue that that came up during the this research was that when XRD is used to estimate the dislocation density in GaN films, the entire volume of the film is included in the analysis. Clearly only dislocations near the surface of the wafer will affect LED performance and a technique that counts only dislocations at the surface is desired. Recently, using a silicon nitride decoration technique (J. Crystal Growth 289, 506 (2006)), AFM images have shown larger pit sizes for screw and mixed dislocations and smaller pit sizes for edge dislocations. The reason for the enhanced identification of dislocations with AFM after coating the GaN surface with silicon nitride is not well understood.

In the remaining time on the project we conducted additional growth runs on the 18 hour annealed sapphire wafers to achieve our $1.0x10^8$ cm^{-2} dislocation density milestone for this project. In addition, the dislocation density was evaluated in two ways; using the XRD technique that we have previously used and the AFM identification technique using the silicon nitride treatment on various samples listed in Table II.

Table II.

XRD and AFM estimates of the dislocation density for GaN on regular and annealed sapphire. The dislocation density estimates that reach Milestone 3.2 are shown in red.

Growth run	XRD screw component $x10^8$ cm^{-2}	XRD edge component $x10^8$ cm^{-2}	AFM screw & mixed dislocations $x10^8$ cm^{-2}	AFM edge dislocations $x10^8$ cm^{-2}
Standard two step GaN growth on sapphire				
DNZ01801 standard growth	4.90	14.0	1.55	2.04
DNZ01806 delayed recovery*	2.97	5.23	2.04	3.68
DNZ01865 delayed recovery	3.56	6.16	1.75	1.22
GaN on annealed sapphire wafers				
DNZ01831 (4 images)	1.64	2.43	0.56	0.58
DNZ01836 (11 images)	3.14	1.55	0.58	0.60
DNZ01871 (5 images)	3.13	2.91	1.02	0.98
DNZ01883 (4 images)	2.80	3.54	0.31	0.50

*silicon nitride treatment conducted by Qiming Li and George Wang in another GaN MOCVD reactor at Sandia as part of an independent evaluation of dislocation density

In Table II are shown dislocation density estimates for standard two step GaN growths (top of the table) and for growth on the annealed sapphire wafers using multiple GaN nucleation layers (bottom of the table). Before AFM imaging the GaN surface was silicon nitride coated to aid in the identification of edge dislocations, since the screw and mixed dislocations are usually observable from the pit formed at the intersection point of two step edges. Fig. 25 illustrates the AFM dislocation counting technique. In Fig. 25(a) the height image is shown and in Fig. 25(b) the corresponding amplitude image is shown. In Figs. 25(c) and 1(d) are shown the same image in (a) and (b) except the screw and mixed dislocations are marked within a white circle and the edge dislocations are marked within a black circle. Decoration of the screw and mixed dislocations produce a larger pit size which is observed typically when two step edges join together, while the edge dislocations produce a smaller pit size which is observed along step edges or on the terrace between steps.

As shown in Table II the AFM measured dislocation density estimates are factors of 3 to 10 lower compared to the XRD measurement estimates of the dislocation density. This still may be due to incomplete decoration of the dislocations by the silicon nitride surface treatment of the

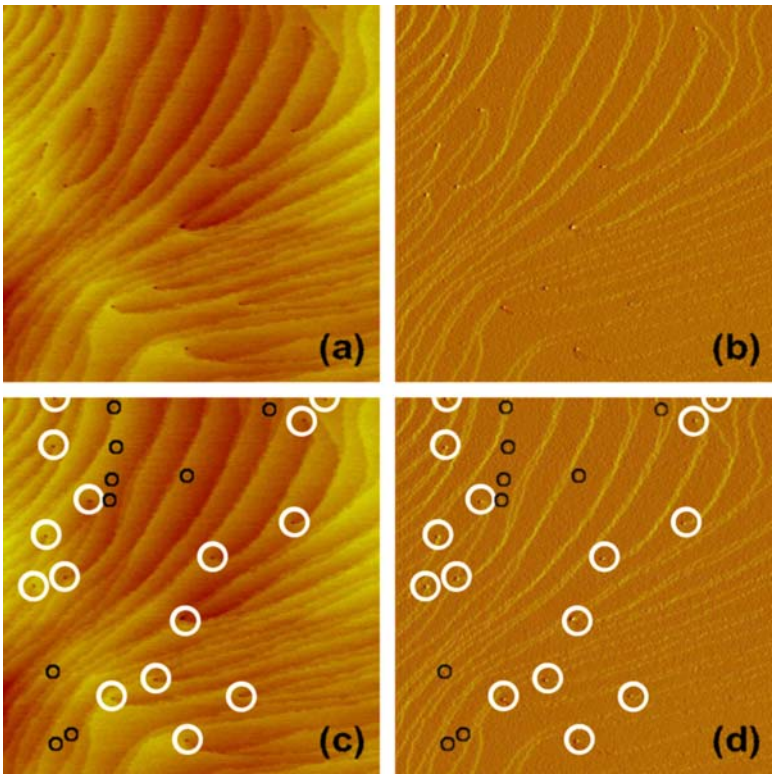

Fig. 25. (a) Height and (b) amplitude AFM images (3 μm x 3 μm) of DNZ01871. In images (c) and (d) the screw and mixed dislocations are circled in white while the edge dislocations are circled in black. Typically, the screw and mixed dislocations are observed as larger holes at the intersection of two step edges, while the edge dislocations are observed as smaller holes located on the terraces or along a step edge.

GaN. To check if this was the case, we used 2 and 4 minute silicon nitride exposure times which both resulted in pits of similar size, suggesting that all of the pits formed by dislocation cores intersecting with the surface are decorated. Similar observations were described previously by Oliver *et al.* (J. Crystal Growth 289, 506 (2006)), where the size of the larger and smaller pits reach a constant size as the silicon nitride treatment time is increased.

Several additional GaN growths on the annealed sapphire wafers were also conducted to further refine the growth process. Dislocation density estimates for two of these growth runs are reported in Table II (growth runs DNZ01871 and DNZ01883). For some of the growth runs the time of the silicon nitride treatment of the sapphire wafer before the growth of the first GaN nucleation was varied, resulting in little change in the overall growth of the films. For a second set of growth runs the number of GaN nucleation layer growth and annealing cycles was varied, resulting in larger coverage of the surface with coalesced GaN when four nucleation layer growth and annealing cycles were used. In a third set of experiments the individual nucleation layer thicknesses were decreased, resulting in a slight improvement in the overall dislocation density with only small regions of the sapphire wafer covered by coalesced GaN.

Using the AFM technique on four 3 μm x 3 μm images we measured screw and mixed dislocation density of 3.1×10^7 cm^{-2} and a edge dislocation density of 5.0×10^7 cm^{-2} for sample DNZ01883 which is shown in Fig. 26, resulting in a total dislocation density 8.1×10^7 cm^{-2} which is less than 1.0×10^8 cm^{-2} dislocation density stated in Milestone 3.2. On this same sample the measured dislocation density using XRD is 2.80×10^8 cm^{-2} for screw component dislocations and 3.54×10^8 cm^{-2} for edge component dislocations. Clearly, more work is needed to determine why the dislocation densities measured by the two

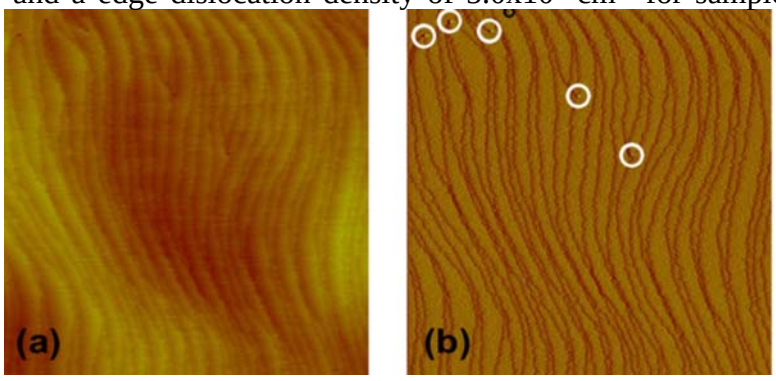

Fig. 26. Same as Fig. 25 with (a) height and (b) amplitude AFM images (3 μm x 3 μm) of DNZ01836. The screw and mixed dislocations are circled in white while the edge dislocations are circled in black.

techniques are significantly different.

4.4 Task 4 summary

Task 4 –Develop full growth model to fit the optical reflectance waveforms during growth.

In March of 2007, work was completed work on deriving the underlying equations that will form the algorithm in the 2-D growth model. In such a model, each crystal face is represented by a line segment that propagates in a given growth direction. Growth rates of different facet types will be calculated based on mass transport from the gas-phase, which may evolve with time. As growth proceeds, facets will grow or shrink in size. Some will disappear or may be overgrown by neighboring facets. We are also hopeful that the same computational approach can be used to describe the initial NL mass loss due to evaporation and subsequent nuclei formation, as well as subsequent growth when the metal-organic precursors are turned on.

In April of 2007, we made a great deal of progress on the morphology evolution computer code. We finished initial coding and debugging of the model. The code now is capable of generating a specified number of initial seed crystals and randomly placing them across the computational domain. The user specifies growth rates of different families of crystal faces, for example the basal plane vs. sloped side-walls. The code then follows the time evolution of the 2-D morphology as the faces evolve. It accounts for the substrate being covered up by the growing film and the evolving crystallite aspect ratios (due to different growth rates on the different face types). During growth some faces "grow to extinction," i.e., disappear as neighboring faces outgrows it. As crystal faces grow into one another some faces disappear, which the code accounts for. The current version of the code has passed all of the initial test problems that have been tried.

We also have written a graphical post-processor to visually inspect the output of the morphology evolution. The post-processor uses a high level graphical package called IDL.

So far, the "growth" portion of the model is working well. However, for the GaN NL evolution problem we also need to consider the evolution of the film as it decomposes during the initial NL heating, mass loss through evaporation, and re-deposition onto more stable crystallites. Upon initial consideration of the problem, we thought that the algorithm and code described above would be general enough to handle this part of the problem. However, it turns out that during the film decomposition, new crystal faces are actually *created* (rather than the situation during growth when faces can only be *destroyed*). In the next month or two we will work on the theory and algorithm that will be needed to describe the film decomposition, and then we will write new code for this part of the NL evolution problem. Unfortunately, due to time restrictions no further progresss was made on simulating the growth.

4.5 Work performed in support of all Tasks

(MOCVD Reactor Move from January to March, 2007)

In January 2007, we were required to shut down our Veeco D-120 MOCVD reactor in order to move it from our previous location in the Compound Semiconductor Research Laboratory (CSRL) to the new Microsystems and Engineering Sciences Applications (MESA) facility. After moving the reactor, outside contractors affiliated with the MESA construction project installed the facilities, including gas lines, electrical, house water, and hazardous process monitoring alarms. This construction was completed in mid-March. During the reactor install, extensive paperwork was processed to ensure compliance with all DOE, Lockheed Martin, and Sandia regulations. This included conducting hazardous barrier analysis (HBA), completion of SEMI-S2 compliance, and sign off on Sandia safety levels 1 and 2 certification before reactor operation could resume.

After the facilities were installed at the end of March, the growth chamber was rebuilt, the entire reactor and gas manifold was leak checked, and alarm shutdowns on the reactor were tested. During the first week of April, Sandia safety level 2 was awarded and some final HPM checks were conducted, after which the ammonia, silane, and hydrogen were turned on for the first time. The source bubblers were also put on the machine. On April 9, we began the first growths in the reactor after the move. To date we have reproduced n-type and p-type GaN films on sapphire and blue wavelength multi-quantum well samples. By April 28th we completed growth runs that verify the operation of the reactor, which includes growth of specular GaN films on sapphire with dislocation densities ~$5x10^{8}$ cm^{-2}, of both n-type and p-type with electron concentrations of ~$5x10^{18}$ cm^{-3} and hole concentrations of ~$5x10^{17}$ cm^{-3}, growth of InGaN/GaN multi-quantum well structures, and growth of light emitting diode (LED) structures. For each of the verification growth runs the design specification were either met or exceeded. For example some of the brightest LEDs ever produced in this Veeco D-125 reactor were produced on the first LED growth run after the move after calibration of the doping levels.

5. Summary of Public Disemmination of Research

For the work performed under this award, we presented our findings at the 7th International Conference on Nitride Semiconductor, held in Las Vegas, NV in September 2007. At this conference we reported on the correlations between the intitial nucleation layer thickness, the resultant nuclei density, and the subsequent dislocation density of the films. It is our intention to publish a Journal of Crystal Growth paper on this presentation in the near future.

We are currently evaluating if any of the growth procedures developed during this work are worthy of filing a patent.

6. References

[1]. W.C. Johnson, J.B. Parsons, M.C. Crew, J. Phys. Chem. 36, 2651 (1932).

[2]. H. Amano, N. Sawaki, I. Akasaki, and Y. Toyoda, "Metalorganic vapor phase epitaxial growth of a high quality GaN film using an AlN buffer layer", Appl. Phys. Lett. 48, 353 (1986).

[3]. S. Nakamura, Jpn. J. Appl. Phys. 30 (1991) L1705.

[4]. D. K. Wickenden, T. J. Kistenmacher, W. A. Bryden, J. S. Morgan, and A. E. Wickenden, Mat. Res. Soc. Symp. Proc. 221 (1991) 167.

[5]. D.D. Koleske, M.E. Coltrin, K.C. Cross, C.C. Mitchell and A.A. Allerman, "Understanding GaN nucleation layer evolution on sapphire", J. Cryst. Growth 273 (2004) 86-99.

[6]. D. D. Koleske, M. E. Coltrin, A. A. Allerman, K. C. Cross, C. C. Mitchell, and J. J. Figiel, "*In situ* measurements of GaN nucleation layer decompostion", Appl. Phys. Lett. 82 (2003) 1170.

[7]. Y**.** Honda, Y**.** Iyechika, T**.** Maeda, H**.** Miyake and K**.** Hiramatsu, "Transmission Electron Microscopy Investigation of Dislocations in GaN Layer Grown by Facet-Controlled Epitaxial Lateral Overgrowth", Jpn. J. Appl. Phys., Part 2, 40, L309-L312 (2001).

[8]. D. M. Follstaedt, P. P. Provencio, N. A. Missert, C. C. Mitchell, D. D. Koleske, A. A. Allerman, and C. I. H. Ashby, "Minimizing threading dislocations by redirection during cantilever epitaxial growth of GaN", Appl. Phys. Lett. 81, 2758 (2002).

[9]. M. E. Coltrin and C. C. Mitchell, "Mass transport and kinetic limitations in MOCVD selective-area growth" J. Cryst. Growth 254, 35-45 (2003).

[10]. M. E. Coltrin and C. C. Mitchell, "Scaling relationships for analyzing kinetics in GaN epitaxial lateral overgrowth", J. Cryst. Growth 261, 30-37 (2004).

[11]. X. H. Wu, P. Fini, E. J. Tarsa, B. Heying, S. Keller, U. K. Mishra, S. P. DenBaars and J. S. Speck, "Dislocation generation in GaN heteroepitaxy , J. Cryst. Growth 189-190, 231-243 (1998).
[12]. T. Hashimoto, M. Yuri, M. Ishida, Y. Terakoshi, O. Imafuji, T. Sugino, and K. Itoh, "Reduction of Threading Dislocations in GaN on sapphire by buffer layer annealing in low-pressure metalorganic chemical vapor deposition", Jpn. J. Appl. Phys. Part 1 38 (1999) 6605.
[13]. B. Moran, F. Wu, A. E. Romanov, U. K. Mishra, S. P. Denbaars, and J. S. Speck, "Structural and morphological evolution of GaN grown by metalorganic chemical vapor deposition on SiC substrates using an AlN initial layer", J. Cryst. Growth 273, 38 (2004).
[14]. D. D. Koleske, A. E. Wickenden, R. L. Henry, M. E. Twigg, J. C. Culbertson, and R. J. Gorman, "Enhanced GaN decomposition in H_2 near atmospheric pressures", Appl. Phys. Lett. 73, 2018 (1998).
[15]. N. D. Bassim, M. E. Twigg, C. R. Eddy, Jr., J. C. Culbertson, M. A. Mastro, R. L. Henry, R. T. Holm, P. G. Neudeck, A. J. Trunek, and J. A. Powell, "Lowered dislocation densities in uniform GaN layers grown on step-free (0001) 4H-SiC mesa surfaces", Appl. Phys. Lett. 86, 021902 (2005).
[16]. D.D. Koleske, M.E. Coltrin and M.J. Russell, "Using optical reflectance to measure GaN nucleation layer decomposition kinetics", J. Cryst. Growth 279, 37-54 (2005).
[17]. D. D. Koleske, A. J. Fischer, A. A. Allerman, C. C. Mitchell, K. C. Cross, S. R. Kurtz, J. J. Figiel, K. W. Fullmer, and W. G. Breiland, "Improved brightness of 380 nm GaN light emitting diodes through intentional delay of the nucleation island coalescence", Appl. Phys. Lett. 81 (2002) 1940.
[18]. R. S. Balmer, C. Pickering, A. J. Pidduck and T. Martin, "Modelling of high temperature optical constants and surface roughness evolution during MOVPE growth of GaN using in-situ spectral reflectometry", J. Cryst. Growth 245, 198-206 (2002).
[19]. S. R. Lee, A. M. West, A. A. Allerman, K. E. Waldrip, D. M. Follstaedt, P. P. Provencio, D. D. Koleske, and C. R. Abernathy, "Effect of threading dislocations on the Bragg peakwidths of GaN, AlGaN, and AlN heterolayers", Appl. Phys. Lett. 86, 241904 (2005).
[20]. T. Lang, M. A. Odnoblyudov, V. E. Bougrov, A. E. Romanov, S. Suihkonen, M. Sopanen, H. Lipsanen**, "**Multistep method for threading dislocation density reduction in MOCVD grown GaN epilayers", Phys. Stat. Sol. (a) 203, R76-R78, (2006).

Appendix A. Brief Project Award Information

1 **DOE Award Number:** M6643033

2 **Project Title:** Nanostructural Engineering of Nitride Nucleation Layers for GaN Substrate Dislocation Reduction

3 **Performer:** Sandia National Laboratories, New Mexico

4 **Principal Investigator: Daniel D. Koleske**
Principal Member of the Technical Staff (PMTS)
Sandia National Laboratories, New Mexico
PO Box 5800
Albuquerque, NM 87185-1086
Phone Number: 505-284-4531 Fax Number: 505-844-3211
E-Mail: ddkoles@sandia.gov

5 **Other Team Members:**
Michael E. Coltrin Sandia National Laboratories, New Mexico
Stephen R. Lee Sandia National Laboratories, New Mexico

6 **Technology Focus:**
Nanotechnology

7 **Relevant Subtask Priority Area:**
High-Efficiency Semiconductor Materials, 1.1.2 (Improve IQE across the visible spectrum and in the near UV – down to 360 nm)

8 **Schedule/Budget Overview:**

	Start Date	End Date	Government Share	Performer Share	Total
Budget Period 1	(10/15/06)	(10/14/07)	$400,000	$ 0	$400,000
Budget Period 2	(10/15/07))	(04/15/08)	$205,000	$ 0	$205,000
Total	**(10/15/06)**	**(04/15/08)**	**$605,000**	**$ 0**	**$605,000**

Distribution:

1	MS1086	Daniel D. Koleske	1126
1	MS1086	Michael E. Coltrin	1126
1	MS1086	Karen C. Cross	1126
1	MS1086	Andrew A. Allerman	1126
1	MS1086	Robert M. Biefeld	1126
1	MS1086	Jeffrey J. Figiel	1126
1	MS1086	Stephen R. Lee	1123
1	MS1086	Mary H. Crawford	1123
1	MS0614	Michael J. Russell	2546
1	MS1084	Thomas K. Lemp	017461
1	MS0899	Technical Library	9536 (electronic copy)